



LAWRENCE
LIVERMORE
NATIONAL
LABORATORY

Benchmark Measurements of the BeRP Ball in Various Reflectors

S. Walston, J. Burch, M. Cowan, G. Guethlein, G.
Keefer, P. Kerr, D. McAvoy, L. Nakae, M. Prasad, D.
Pugh, G. Slavik, N. Snyderman

September 24, 2014

Disclaimer

This document was prepared as an account of work sponsored by an agency of the United States government. Neither the United States government nor Lawrence Livermore National Security, LLC, nor any of their employees makes any warranty, expressed or implied, or assumes any legal liability or responsibility for the accuracy, completeness, or usefulness of any information, apparatus, product, or process disclosed, or represents that its use would not infringe privately owned rights. Reference herein to any specific commercial product, process, or service by trade name, trademark, manufacturer, or otherwise does not necessarily constitute or imply its endorsement, recommendation, or favoring by the United States government or Lawrence Livermore National Security, LLC. The views and opinions of authors expressed herein do not necessarily state or reflect those of the United States government or Lawrence Livermore National Security, LLC, and shall not be used for advertising or product endorsement purposes.

This work performed under the auspices of the U.S. Department of Energy by Lawrence Livermore National Laboratory under Contract DE-AC52-07NA27344.

Benchmark Measurements of the BeRP Ball in Various Reflectors

Sean Walston,^{a)} Jennifer Burch, Matt Cowan, Gary Guethlein, Greg Keefer, Phil Kerr, Doug McAvoy, Les Nakae, Manoj Prasad, Darrell Pugh, Gary Slavik, and Neal Snyderman
Lawrence Livermore National Laboratory, Livermore, California^{b)}

(Dated: 7 August 2014)

Details of benchmark neutron multiplicity measurements of the 4.484 kg Beryllium Reflected Plutonium (BeRP) ball inside of various reflectors. Measurements were performed with an Ortec Fission Meter neutron multiplicity counter. Measurements were made of the bare BeRP Ball, the BeRP Ball inside 3 inch thick polyethylene, nickel, and tungsten, and the polyethylene with an additional 2 inch thick steel reflector. For every measurement, the mass m_S of ^{240}Pu , k_{eff} , multiplication M , and escape multiplication M_E are reported. For each individual measurement, the measured mass m_S of ^{240}Pu in the BeRP Ball was within 20.7 grams (closest edge of measurement errorbar to closest edge of errorbar for reference m_S from isotopics). The combined measurement of the mass of ^{240}Pu $m_S = 267 \pm 7$ grams which compared very favorably to the known value from isotopics of $m_S = 266.8 \pm 0.5$ grams.

I. INTRODUCTION

These subcritical experiments with the Beryllium Reflected Plutonium (BeRP) ball inside of nickel and tungsten reflectors measured the mass of the ^{240}Pu m_S in the BeRP Ball and the resulting multiplication M where

$$M = \frac{1}{1 - k_{\text{eff}}} \quad (1)$$

$$M_E = \frac{1 - p}{1 - k_{\text{eff}}} \quad (2)$$

The quantity $k_{\text{eff}} = \bar{\nu}p$ where p is the probability that a free neutron induces a fission in a ^{239}Pu atom and $\bar{\nu}$ is the average number of neutrons created by an induced fission of ^{239}Pu . The BeRP Ball is a 4.484 kg sphere of α -phase plutonium.¹

II. EXPERIMENT

Experiments were performed with an ORTEC Fission Meter²⁻⁴ (Serial Number FMP1). The Fission Meter was oriented upright in the folded or open configurations. In the folded configuration, the ^3He tubes were facing outward and the high-density polyethylene (poly) moderator was sandwiched between the rows of tubes. This is referred to as the “tubes-poly-poly-tubes” or “TPPT” configuration. The front face of the Fission Meter was the specified distance from the center of the BeRP Ball. In the open configuration, the tubes faced the BeRP Ball and the perpendicular distance from the center of each panel was equidistant to the center of the BeRP Ball.

The digital outputs of each channel of the Fission Meter were connected to a “time tagger suitcase” which was a system that logged the arrival time of each neutron to create time-tagged list-mode data.

This time-tagged data was then analyzed by breaking the observation time up into successive time gates T and counting the number of neutrons detected within each. For each value of T , a multiplicity histogram was created. Suppose in an experiment, N time gates of duration T were examined, and let $B_n(T)$ be the number of those time gates in which n neutrons were detected. So for example, suppose that during the first time gate, four neutrons were counted; B_4 would be incremented by one. During the next time gate, say two neutrons were counted; B_2 would be incremented by one, and so on for all N time gates of a given duration T . In this way, the count distribution $B_n(T)$ is built up. The probability distribution $b_n(T) \approx B_n(T)/N$ for $N \gg 1$.

This process was then repeated for numerous different values of T in such a way that no neutron was reused in time gates of different values of T . This non-reuse of neutrons procedure avoided difficulties with the unknown covariance between $B_n(T)$ among the various values of n across the different values of T .

The α -phase plutonium sphere, known as the BeRP (Beryllium Reflected Plutonium) ball,¹ weighed approximately 4.484 kg and had a mean diameter of 7.5876 cm.

^{a)}Electronic mail: walston2@llnl.gov

^{b)}This document was prepared as an account of work sponsored by an agency of the United States government. Neither the United States government nor Lawrence Livermore National Security, LLC, nor any of their employees makes any warranty, expressed or implied, or assumes any legal liability or responsibility for the accuracy, completeness, or usefulness of any information, apparatus, product, or process disclosed, or represents that its use would not infringe privately owned rights. Reference herein to any specific commercial product, process, or service by trade name, trademark, manufacturer, or otherwise does not necessarily constitute or imply its endorsement, recommendation, or favoring by the United States government or Lawrence Livermore National Security, LLC. The views and opinions of authors expressed herein do not necessarily state or reflect those of the United States government or Lawrence Livermore National Security, LLC, and shall not be used for advertising or product endorsement purposes.

^{b)} This work performed under the auspices of the U.S. Department of Energy by Lawrence Livermore National Laboratory under Contract DE-AC52-07NA27344.

Total Mass (g)	Isotope	Weight Fraction (%)	Weight of Isotope (g)
4483.884	²³⁸ Pu	0.02	0.9
	²³⁹ Pu	93.735 ± .005	4202.97 ± 0.22
	²⁴⁰ Pu	5.95 ± .01	266.8 ± 0.5
	²⁴¹ Pu	0.2685 ± .0005	12.039 ± 0.022
	²⁴² Pu	0.028	1.3

TABLE I. BeRP Ball specifications.¹

The isotopic details of the BeRP Ball are shown in Table I.

The reflectors were comprised of nesting hemishells which fit around the BeRP Ball. The nested hemishells allowed varying thicknesses. Except for the steel, all reflectors fit tightly around the BeRP Ball. The steel fit tightly around the 3 inch thick polyethylene.

In addition to measurements with the BeRP Ball inside the various reflectors, a ²⁵²Cf source was placed inside the same reflectors to establish the detection efficiency for the given configuration. The Fission Meter was at the same distance and in the same configuration as the corresponding measurement with the BeRP Ball.

$$\mathcal{P}(y) = (1-p)y + y^n \sum_{k=1}^{\infty} \frac{P_p(k|n+k)}{k+n} \sum_{\nu_0, \nu_1, \nu_2, \dots} \frac{k!}{\nu_0! \nu_1! \nu_2! \dots} (C_0^{\nu_0} C_1^{\nu_1} C_2^{\nu_2} \dots) \quad (5)$$

where

$$P_p(k|n+k) = \frac{(k+n)!}{k!n!} p^k (1-p)^n \quad (6)$$

is the binomial distribution⁸ for k “successes” out of $k+n$ trials if the probability of a “success” is p , and where ν_0 is the number of fissions which produce zero neutrons, ν_1 is the number of fissions which produce one neutron, ν_2 the number of fissions which produce two neutrons, and so on. The quantity k here has the interpretation of the total number of fissions in the chain. The probability distribution \mathcal{P}_n that we want are the coefficients on y^n as shown in Eq. 3.

For fission chains initiated by spontaneous fission, it becomes necessary to compute the probability distribution \mathcal{P}_{S_n} which is the probability that a fission chain initiated by a spontaneous fission creates n neutrons. Starting with the probability $C_{S\nu}$ that a spontaneous

III. STATISTICAL THEORY OF FISSION CHAINS

A. Statistical Relationship Between the Neutron Multiplicity Distribution and the Source Parameters

The first piece of the statistical theory of fission chains is the probability \mathcal{P}_n that a fission chain, initiated by a single neutron inducing a fission, creates n neutrons that become available for detection. There is no simple formula for the probabilities \mathcal{P}_n for various values of n , but it is possible instead to give a formula for the sum of a power series whose coefficients are the probabilities \mathcal{P}_n that we’re interested in.⁵ A generating function can be constructed by simply multiplying the probabilities \mathcal{P}_n by x^n and summing over n :

$$\mathcal{P}(x) = \sum_{n=0}^{\infty} \mathcal{P}_n x^n \quad (3)$$

where, throughout, the Feynman-slash notation denotes the generating function corresponding to a probability distribution.

Starting with the probability p that a neutron induces a fission and the probability C_ν that an induced fission in ²³⁹Pu creates ν neutrons, shown in Table II, the generating function for the number of neutrons a fission chain creates satisfies the equation⁶

$$-\mathcal{P}(y) + (1-p)y + p\mathcal{C}'[\mathcal{P}(y)] = 0 \quad (4)$$

The solution to Eq. 4 is⁷

fission in ²⁴⁰Pu creates ν neutrons, shown in Table II, the generating function for the number of neutrons a spontaneous fission-initiated fission chain creates, $\mathcal{P}_S(y)$, can be calculated by repeated application of the convolution theorem.⁷ The generating function $\mathcal{S}(z)$ of the sum of two independent random variables x_1 and x_2 is the product of the generating functions for x_1 and x_2 ; $\mathcal{S}(z) = \mathcal{f}_1(z)\mathcal{f}_2(z)$. For a compound process, the generating function of a sum of a random number of random variables x_1, x_2, \dots, x_n where n is itself a random variable with generating function $\mathcal{h}(z)$ is $\mathcal{h}(\mathcal{S}(z))$. The generating function for the number of neutrons a spontaneous fission-initiated fission chain creates is

$$\mathcal{P}_S(y) = \mathcal{C}'_S(\mathcal{P}(y)) \quad (7)$$

where the generating function $\mathcal{P}(y)$ is substituted in for the argument of the generating function $\mathcal{C}'_S(x)$. Again, the probability distribution \mathcal{P}_{S_n} that we want are the

coefficients on y^n in Eq. 7.

Applying the same logic developed for a compound process again, the probability e_{Sm} of detecting m of the n neutrons created by the spontaneous fission-initiated fission chain is calculated as

$$\phi'_S(y) = \mathcal{P}'_S(\phi(y)) \quad (8)$$

$$= \mathcal{Q}'_S(\mathcal{P}'(\phi(y))) \quad (9)$$

where in the absence of double-pulsing, the generating

function $\phi(y)$ for a detection efficiency of ϵ is

$$\phi(y) = (1 - \epsilon) + \epsilon y \quad (10)$$

The average number of instances of detecting k neutrons from a single fission chain within the time gate T is thus the product of e_{Sm} and Δ_{mk} (summed over m with the Einstein summation convention),

$$\Lambda_k(T) = e_{Sm} \Delta_{mk} \quad (11)$$

where

$$\begin{aligned} \Delta_{mk} &= \binom{m}{k} \left\{ \int_{-\infty}^0 \left[\int_0^T e^{-\lambda(t-s)} \lambda dt \right]^k \left[1 - \int_0^T e^{-\lambda(t-s)} \lambda dt \right]^{m-k} F_S ds \right. \\ &\quad \left. + \int_0^T \left[\int_s^T e^{-\lambda(t-s)} \lambda dt \right]^k \left[1 - \int_s^T e^{-\lambda(t-s)} \lambda dt \right]^{m-k} F_S ds \right\} \\ &= \frac{F_S}{\lambda} \binom{m}{k} B[(1 - e^{-\lambda T}); k, m - k] \end{aligned} \quad (12)$$

is the probability of detecting k out of the total m detected neutrons within the time gate T and where λ is the inverse of the neutron diffusion time.⁹ This is just a binomial distribution where the first term accounts for neutrons created before the time gate T and the second term accounts for neutrons created during the time gate T . The integrals evaluate to an incomplete Beta function $B(z; a, b)$. The term F_S is the rate of spontaneous fissions,

$$F_S = \frac{N_A \ln 2}{A} \frac{t_{1/2}}{t_{1/2}^{\text{SF}}} m_S \quad (13)$$

where m_S is the mass of the spontaneously fissioning isotope (^{240}Pu in this case). The half-life was taken to be $t_{1/2} = 6562.8$ years and the half-life against spontaneous fission was taken as $t_{1/2}^{\text{SF}} = 1.151 \times 10^{11}$ years.

The multiplicity distribution $b_j(T)$ can be computed from the $\Lambda_k(T)$ with the generating function

$$\mathcal{P}(z) = e^{[\sum_{k=1}^{\infty} (z^k - 1) \Lambda_k]} \quad (14)$$

along with a choice for the duration of the time gate T and knowledge of the inverse of the neutron diffusion time λ .

The resulting values for $b_n(T)$ were then compared to the measured count distributions $B_n(T)$ to optimize the system's remaining parameters k_{eff} , ϵ , and m_S using the method of least squares,

$$\chi^2 = \sum_{T, B_n \neq 0} \frac{(B_n - N b_n)^2}{N b_n} \quad (15)$$

where the sum ran over values of T and $B_n(T) \neq 0$. The system parameters k_{eff} , ϵ , and m_S were taken as those that minimized $\chi^2 \rightarrow \chi^2_{\text{min}}$.

It can be shown that even if the resulting χ^2 does not follow the usual χ^2 distribution as a function of the parameters, the central confidence interval can still be approximated by using

$$\chi^2(\theta_{-\sigma}^{+\sigma}) = \chi^2_{\text{min}} + \Delta\chi^2 \quad (16)$$

where θ is the vector of parameters k_{eff} , ϵ , and m_S .^{10,11} The value of $\Delta\chi^2$ was taken as^{10,11}

$$\Delta\chi^2 = F_{\chi^2}^{-1} \left(1 - \text{erf} \left(\sqrt{2}^{-1} \right), n_{\text{DOF}} \right) \quad (17)$$

where $F_{\chi^2}^{-1}$ is the inverse of the cumulative distribution for the χ^2 distribution and where erf is the error function which, with an argument of $\sqrt{2}^{-1}$, gives the usual 1σ probability of 68.27% confidence. The quantity n_{DOF} was the number of degrees of freedom which was equal to the number of values of $B_n(T) \neq 0$ minus three for the three remaining system parameters we desired, k_{eff} , ϵ , and m_S .

The parameter space of k_{eff} , ϵ , and m_S was explored to locate $\widehat{k_{\text{eff}}}$, $\widehat{\epsilon}$, and $\widehat{m_S}$ that correspond to χ^2_{min} . In addition, the parameter space was explored to find those values of k_{eff} , ϵ , and m_S corresponding to $\chi^2(\theta_{-\sigma}^{+\sigma}) = \chi^2_{\text{min}} + \Delta\chi^2$.

Comparison of the measured multiplicity distributions to theoretical multiplicity distributions requires prior knowledge of λ .

B. Statistical Relationship Between the Neutron Multiplicity Distribution and λ

The rate of counting j neutrons all coming from the same fission chain can be determined by computing the

$$Y_j(T) = \sum_{n=j}^{\infty} \mathcal{P}_{S_n} \binom{n}{j} \epsilon^j F_S \left\{ \frac{(1 - e^{-\lambda T})^j}{\lambda j} + T - \frac{1}{\lambda} \sum_{n=0}^{j-1} B[(1 - e^{-\lambda T}); j - n, 1] \right\} \quad (19)$$

where $B(z; a, b)$ is the incomplete beta function.¹² We can define the leading terms to be

$$R_j = \sum_{n=j}^{\infty} \mathcal{P}_{S_n} \binom{n}{j} \epsilon^j F_S \quad (20)$$

resulting in

$$Y_1(T) = R_1 T \quad (21)$$

$$Y_2(T) = R_2 \left(T - \frac{1 - e^{-\lambda T}}{\lambda} \right) \quad (22)$$

It is convenient to define

$$Y_{2F} = \frac{Y_2}{Y_1} \quad (23)$$

$$R_{2F} = \frac{R_2}{R_1} \quad (24)$$

Applying Eqs. 21 and 22, the quantity of interest is found to be^{13–16}

$$Y_{2F}(T) = R_{2F} \left(1 - \frac{1 - e^{-\lambda T}}{\lambda T} \right) \quad (25)$$

To extract the rates $Y_j(T)$ experimentally from a measured count distribution $B_n(T) \approx N b_n(T)$ for $N \gg 1$ randomly-triggered time gates of length T requires the combinatorial moments of the count distribution,

$$\mathcal{M}_j(T) = \frac{1}{N} \sum_{n=j}^{\infty} \binom{n}{j} B_n(T) \quad (26)$$

These can be computed from the generating function $\mathcal{b}(z)$, Eq. 14, as

$$\mathcal{M}_j = \frac{1}{j!} \left. \frac{d^j \mathcal{b}}{dz^j} \right|_{z=1} \quad (27)$$

combinatorial moments of the $\Lambda_k(T)$,

$$Y_j(T) = \sum_{k=j}^{\infty} \binom{k}{j} \Lambda_k(T) \quad (18)$$

An explicit form for $Y_j(T)$ is obtained by substituting Eq. 11 into Eq. 18,

The \mathcal{M}_j for $j = 1, 2$ expressed in terms of the Λ_k are

$$\mathcal{M}_1 = \sum_{k=1}^{\infty} \binom{k}{1} \Lambda_k \quad (28)$$

$$= Y_1 \quad (29)$$

$$\mathcal{M}_2 = \sum_{k=2}^{\infty} \binom{k}{2} \Lambda_k + \frac{1}{2!} \left[\sum_{k=1}^{\infty} \binom{k}{1} \Lambda_k \right]^2 \quad (30)$$

$$= Y_2 + \frac{Y_1^2}{2!} \quad (31)$$

Solving for Y_1 and Y_2 in terms of \mathcal{M}_1 and \mathcal{M}_2 yields

$$Y_1 = \mathcal{M}_1 \quad (32)$$

$$Y_2 = \mathcal{M}_2 - \frac{\mathcal{M}_1^2}{2!} \quad (33)$$

leading to

$$Y_{2F}(T) = \frac{\mathcal{M}_2(T)}{\mathcal{M}_1(T)} - \frac{\mathcal{M}_1(T)}{2!} \quad (34)$$

As a practical matter, the combinatorial moments \mathcal{M}_j of the counting distribution $B_n(T)$ are easy to compute from Eq. 26.

The quantities λ and R_{2F} are determined by minimizing

$$\chi^2 = \mathbf{E}_{2F}^T W^{-1} \mathbf{E}_{2F} \quad (35)$$

where the superscript T denotes transpose and where the error vector \mathbf{E}_{2F} is defined as

$$\mathbf{E}_{2F} = \frac{\mathcal{M}_2(T_i)}{\mathcal{M}_1(T_i)} - \frac{\mathcal{M}_1(T_i)}{2!} - R_{2F} \left(1 - \frac{1 - e^{-\lambda T_i}}{\lambda T_i} \right) \quad (36)$$

and is understood to be a column vector corresponding to the values for T_i . The covariance matrix W depends on how the different values of T are chosen: we have avoided using the same neutron counts to populate count distributions with different values of T so that W will be

C. Statistical Relationship Between the Neutron Multiplicity Distribution for ^{252}Cf and the Detection Efficiency

Given a neutron multiplicity distribution for spontaneous fission $\mathcal{P}_{S\nu} \rightarrow C_{S\nu}$ for ^{252}Cf shown in Table II, we find from Eq. 20 that

$$R_{2F} = \epsilon \times \bar{\nu}_2 / \bar{\nu}_1 \quad (49)$$

Let the combinatorial moments of $C_{S\nu}$ be

$$\bar{\nu}_j = \sum_{n=j}^{\infty} C_{S\nu} \binom{\nu}{j} \quad (50)$$

For a particular measurement using ^{252}Cf , once a value for R_{2F} was obtained from the minimization of Eq. 35, it was then a simple matter to compute the detection efficiency ϵ from Eq. 49. Using an average of three measurements for $C_{S\nu}$ ¹⁸⁻²⁰, shown in Table II, the ratio $\bar{\nu}_2 / \bar{\nu}_1 = 1.5930 \pm 0.0030$. This uncertainty was included in the error on the detection efficiency ϵ .

IV. RESULTS

Results for measurements of the detection efficiency ϵ determined using ^{252}Cf are shown in Table III. Measurements of the neutron diffusion time λ^{-1} with the BeRP Ball are shown in Table IV. Results of these benchmark measurements are shown in Table V.

For each experiment, the first figure shows Y_{2F} vs. time gate T for the ^{252}Cf source that was used to determine the detection efficiency ϵ . The second figure shows Y_{2F} vs. time gate T for the BeRP Ball in the corresponding configuration used to determine the diffusion time λ^{-1} . The third figure shows the measured mass m_S of the ^{240}Pu after applying the measured detection efficiency ϵ determined from the measurement with the ^{252}Cf source. The statistical error is shown separately from the error that resulted from the determination of the diffusion time λ^{-1} . The fourth figure shows the measured multiplication M after applying the measured detection efficiency ϵ determined from the measurement with the ^{252}Cf source. Again, the statistical error is shown separately from the error that resulted from the determination of the diffusion time λ^{-1} . The fifth figure shows a comparison of the measured and theoretical multiplicity distributions for the example of $T = 500 \mu\text{s}$. The sixth figure shows the multiplication M vs. mass m_S of ^{240}Pu determined from the measurement. The error shown includes all enumerated sources of uncertainty. The true value of the mass m_S of ^{240}Pu is shown for comparison.

A. Averaging and Treatment of Errors

When multiple measurements were made with the same source configuration, the resulting measurements

were then averaged using the procedure adopted by the Particle Data Group for the Review of Particle Physics.¹⁰ A weighted average and error were calculated as

$$\bar{x} \pm \sigma_x = \frac{\sum_i w_i x_i}{\sum_i w_i} \pm \sqrt{\sum_i w_i} \quad (51)$$

where

$$w_i = \frac{1}{\sigma_{x_i}^2} \quad (52)$$

and where $x_i \pm \sigma_{x_i}$ were the value and error for the i th measurement. The sums ran over the N measurements for a particular source configuration. A χ^2 was then calculated in the usual way as

$$\chi^2 = \sum_i w_i (\bar{x} - x_i)^2 \quad (53)$$

and compared to $N - 1$, the expectation value of χ^2 if the measurements were Gaussian-distributed.

- If $\chi^2 / (N - 1) \leq 1$, the results were accepted.
- If $\chi^2 / (N - 1) > 1$, the quoted error σ_x was increased by a scale factor S defined as

$$S = \sqrt{\frac{\chi^2}{N - 1}} \quad (54)$$

with the reasoning that the large value of χ^2 was likely to be due to an underestimation of the errors in at least one of the measurements. Not knowing which of the errors were underestimated, it was assumed they were all underestimated by the same factor S . By scaling up all the input errors σ_{x_i} by this factor, the χ^2 then became $N - 1$. Of course the output error σ_x scaled up by the same factor. Because measurements could be made with widely-varying count times, the corresponding errors could also be widely varying. The scale factor S was thus evaluated using only the measurements with errors $\sigma_{x_i} \leq 3\sigma_x \sqrt{N}$. The reasoning was that, although the low-precision measurements have little influence on the values x and σ_x , they can make significant contributions to χ^2 thus obscuring the contribution of the high-precision measurements.¹⁰

This scaling procedure has the property that if there are two values with comparable errors separated by much more than their stated errors, the scaled-up error turns out to be roughly half the interval between the two discrepant values. It also in no way affects the central value. And if one wishes to recover the unscaled error, one can simply divide the quoted error by S .

The average values for the measured mass of ^{240}Pu m_S , k_{eff} , multiplication M , and escape multiplication M_E for each source configuration are shown in Table VI.

Reflector	Thickness (inches)	Dist. (cm)	Detector Config.	Count Time (s)	Count Rate (n/s)	R_{2F}	λ^{-1} (μ s)	ϵ (^{252}Cf) (%)	χ^2	n_{DOF}
None	0	25	Open	328	1122.4 ± 1.8	0.0177 ± 0.0025	140 ± 70	1.11 ± 0.16	2.5	6
None	0	30	TPPT	309	1459.6 ± 2.2	0.018 ± 0.0025	130 ± 70	1.13 ± 0.16	4.6	6
Polyethylene	3	25	Open	305	5637 ± 4	0.0608 ± 0.0028	153 ± 18	3.81 ± 0.18	5.8	6
Polyethylene, Steel	3, 2	25	Open	3663	1475.8 ± 0.6	0.0161 ± 0.0006	83 ± 15	1.01 ± 0.04	10.8	6
Steel	2	25	Open	411	1692.8 ± 2	0.0226 ± 0.0018	70 ± 40	1.42 ± 0.12	5.8	6
Nickel	3	30	TPPT	547	1948.5 ± 1.9	0.0268 ± 0.0021	171 ± 33	1.68 ± 0.13	8.4	6
Nickel	3	50	TPPT	452	995.6 ± 1.5	0.0087 ± 0.0014	0 ± 0	0.55 ± 0.09	8.4	6
Tungsten	3	29	TPPT	609	2221 ± 1.9	0.0227 ± 0.0015	60 ± 32	1.43 ± 0.09	7.6	6
Tungsten	3	49	TPPT	637	1093.2 ± 1.3	0.0158 ± 0.0021	200 ± 60	0.99 ± 0.13	2.3	6

TABLE III. Measurements of the ^{252}Cf in various reflectors. The detection efficiency ϵ was determined from the fits to R_{2F} from measurements of ^{252}Cf in the same reflector with the Fission Meter at the same distance and in the same configuration (tubes-poly-poly-tubes — “TPPT,” or “Open”).

Reflector	Thickness (inches)	Dist. (cm)	Detector Config.	Count Time (s)	Count Rate (n/s)	R_{2F}	λ^{-1} (μ s)	χ^2	n_{DOF}
None	0	25	Open	363	7890 ± 5	0.1551 ± 0.0023	47 ± 6	1.9	6
None	0	30	TPPT	454	11269 ± 5	0.2211 ± 0.0024	73 ± 4	2.9	6
Polyethylene	3	25	Open	1016	116962 ± 11	7.809 ± 0.021	263.5 ± 1.2	19.7	6
Polyethylene, Steel	3, 2	25	Open	1004	32663 ± 6	2.132 ± 0.007	185.2 ± 1.3	6.5	6
Polyethylene, Steel	3, 2	25	Open	1217	33054 ± 5	2.163 ± 0.006	186.8 ± 1.1	11.5	6
Steel	2	25	Open	1706	11522.7 ± 2.6	0.2402 ± 0.0012	38.5 ± 1.8	3.4	6
Nickel	3	30	TPPT	488	31574 ± 8	1.619 ± 0.008	78.6 ± 1.7	6.2	6
Nickel	3	50	TPPT	647	15711 ± 5	0.786 ± 0.004	77 ± 1.8	2.2	6
Tungsten	3	29	TPPT	312	43391 ± 12	2.75 ± 0.016	75.7 ± 2	8.9	6
Tungsten	3	49	TPPT	312	21640 ± 8	1.374 ± 0.009	84.1 ± 2.3	2.0	6

TABLE IV. Measurements of the BeRP Ball in various reflectors. The neutron diffusion time λ^1 was determined from the fits to R_{2F} . This quantity then fed into the fits of the multiplicity distributions to determine the measured mass of ^{240}Pu m_S and k_{eff} .

Reflector	Thickness (inches)	Dist. (cm)	Detector Config.	ϵ (^{252}Cf) (%)	m_S (g)	k_{eff}	M	M_E	χ^2	n_{DOF}
None	0	25	Open	1.11 ± 0.16	232 ± 26	0.756 ± 0.029	4.1 ± 0.5	3.07 ± 0.32	2493	141
None	0	30	TPPT	1.13 ± 0.16	277 ± 29	0.793 ± 0.022	4.8 ± 0.5	3.56 ± 0.34	1677	178
Polyethylene	3	25	Open	3.81 ± 0.18	269 ± 12	0.9380 ± 0.0033	16.1 ± 0.8	11.1 ± 0.6	4380	2040
Polyethylene, Steel	3, 2	25	Open	1.01 ± 0.04	282 ± 9	0.9382 ± 0.0021	16.2 ± 0.6	11.1 ± 0.4	2060	628
Polyethylene, Steel	3, 2	25	Open	1.01 ± 0.04	282 ± 13	0.9381 ± 0.0034	16.2 ± 0.9	11.1 ± 0.6	3927	566
Steel	2	25	Open	1.42 ± 0.12	239 ± 13	0.776 ± 0.012	4.46 ± 0.24	3.31 ± 0.16	297	206
Nickel	3	30	TPPT	1.68 ± 0.13	244 ± 15	0.907 ± 0.006	10.7 ± 0.7	7.5 ± 0.5	661	635
Nickel	3	50	TPPT	0.55 ± 0.09	311 ± 31	0.925 ± 0.008	13.3 ± 1.4	9.2 ± 0.9	360	350
Tungsten	3	29	TPPT	1.43 ± 0.09	282 ± 18	0.934 ± 0.005	15.3 ± 1.1	10.5 ± 0.7	729	1021
Tungsten	3	49	TPPT	0.99 ± 0.13	239 ± 22	0.923 ± 0.008	13.0 ± 1.3	9.0 ± 0.9	460	495

TABLE V. Measurements of the BeRP Ball in various reflectors. The detection efficiency ϵ was determined from a measurement of ^{252}Cf in the same reflector with the Fission Meter at the same distance and in the same configuration (tubes-poly-poly-tubes — “TPPT,” or open). The detection efficiency ϵ , the measured mass of ^{240}Pu m_S , k_{eff} , multiplication M , and the escape multiplication M_E are listed in the table.

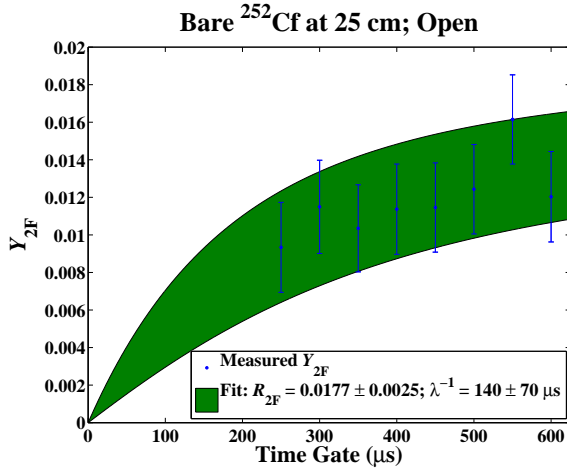


FIG. 1. Y_{2F} vs. time gate T for bare ^{252}Cf 25 cm from the detector. The green contour represents the 1σ errors (68.3% confidence region) in the measurements.

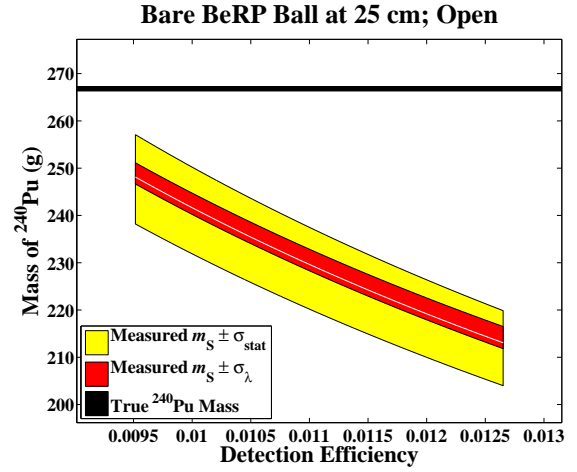


FIG. 3. Mass m_S of ^{240}Pu vs. detection efficiency ϵ for the bare BeRP Ball 25 cm from the detector. The yellow contour represents the 1σ statistical errors (68.3% confidence region) in the measurements for the central value of λ . The red contour represents the 1σ errors in the measurements due to the measured error in λ . The central value is noted by the white curve. The true mass of $^{240}\text{Pu} = 266.8 \pm 0.5$ g and is indicated by the black horizontal line in the plot.

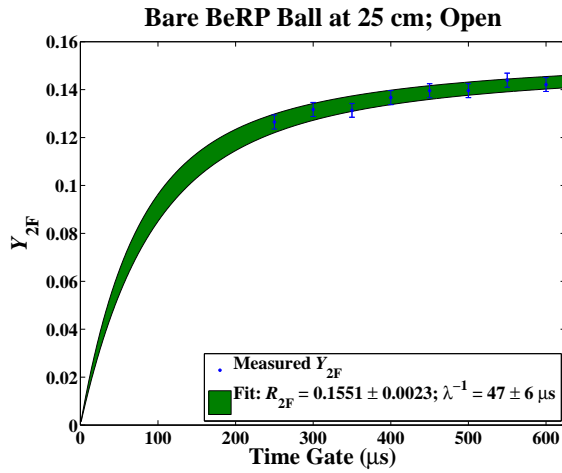


FIG. 2. Y_{2F} vs. time gate T for the bare BeRP Ball 25 cm from the detector. The green contour represents the 1σ errors (68.3% confidence region) in the measurements.

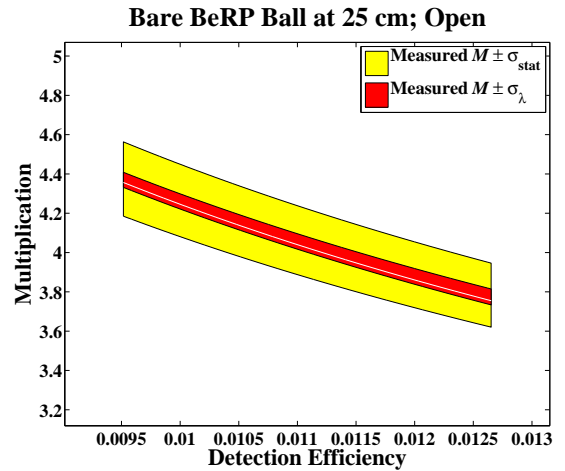


FIG. 4. Multiplication M vs. detection efficiency ϵ for the bare BeRP Ball 25 cm from the detector. The yellow contour represents the 1σ statistical errors (68.3% confidence region) in the measurements for the central value of λ . The red contour represents the 1σ errors in the measurements for the measured error in λ . The central value is noted by the white curve.

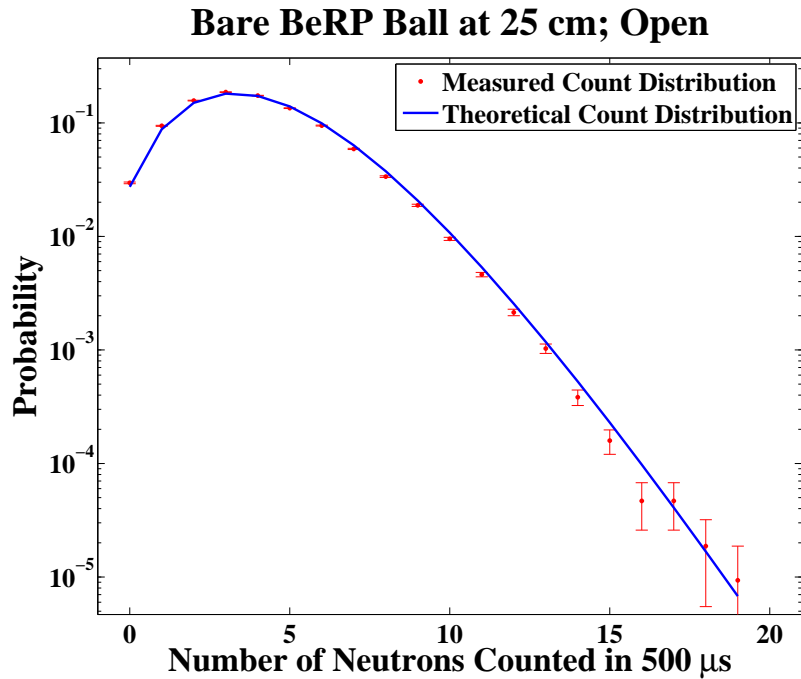


FIG. 5. Probability of counting n neutrons in a randomly-triggered time gate of duration $T = 500 \mu\text{s}$ for the bare BeRP Ball 25 cm from the detector.

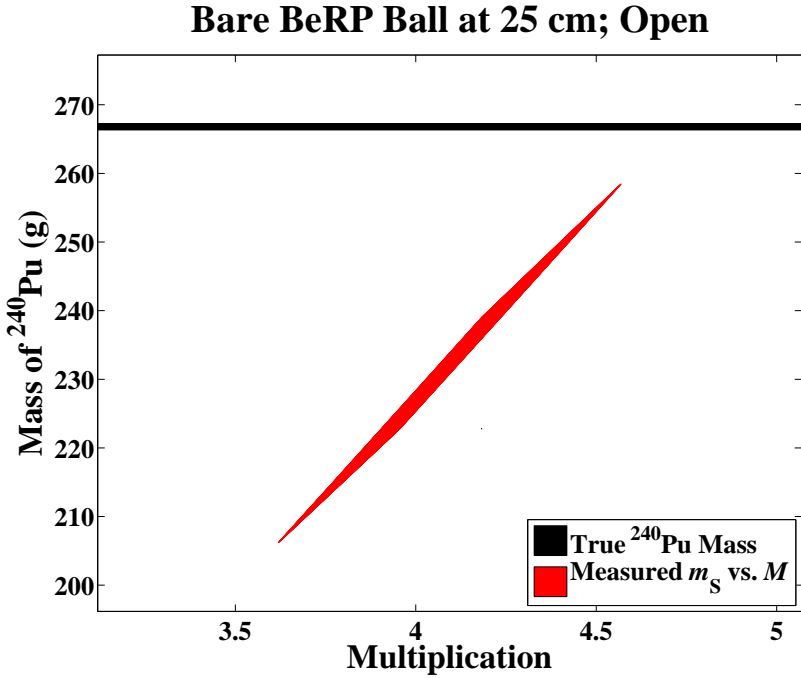


FIG. 6. Multiplication M vs. mass of ^{240}Pu for the bare BeRP Ball 25 cm from the detector. The red trapezoidal contour represents the 1σ error (68.3% confidence region) in the measurement. The true mass of $^{240}\text{Pu} = 266.8 \pm 0.5 \text{ g}$ and is indicated by the black horizontal line in the plot.

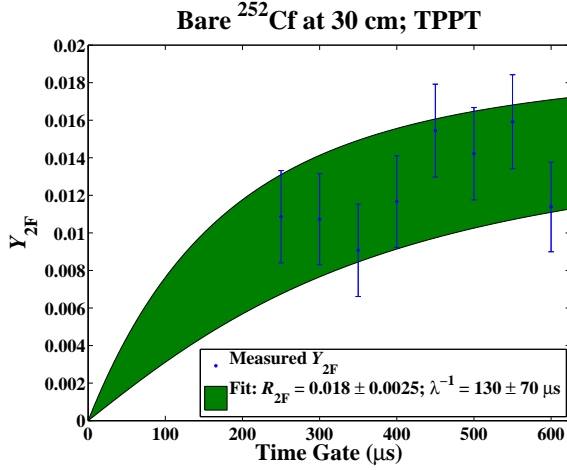


FIG. 7. Y_{2F} vs. time gate T for bare ^{252}Cf 30 cm from the detector. The green contour represents the 1σ errors (68.3% confidence region) in the measurements.

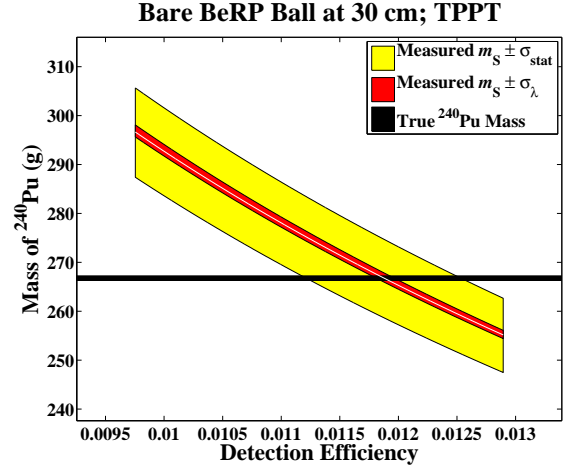


FIG. 9. Mass m_S of ^{240}Pu vs. detection efficiency ϵ for the bare BeRP Ball 30 cm from the detector. The yellow contour represents the 1σ statistical errors (68.3% confidence region) in the measurements for the central value of λ . The red contour represents the 1σ errors in the measurements due to the measured error in λ . The central value is noted by the white curve. The true mass of $^{240}\text{Pu} = 266.8 \pm 0.5$ g and is indicated by the black horizontal line in the plot.

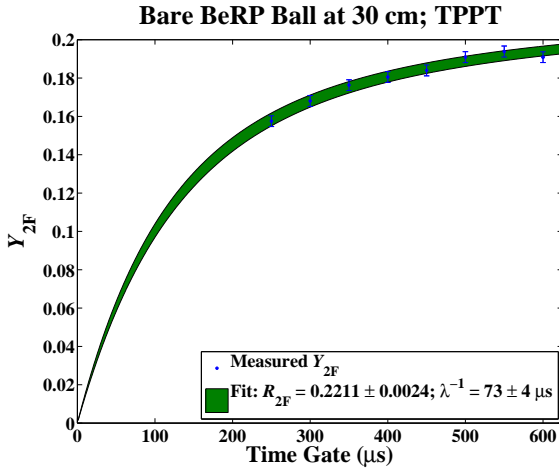


FIG. 8. Y_{2F} vs. time gate T for the bare BeRP Ball 30 cm from the detector. The green contour represents the 1σ errors (68.3% confidence region) in the measurements.

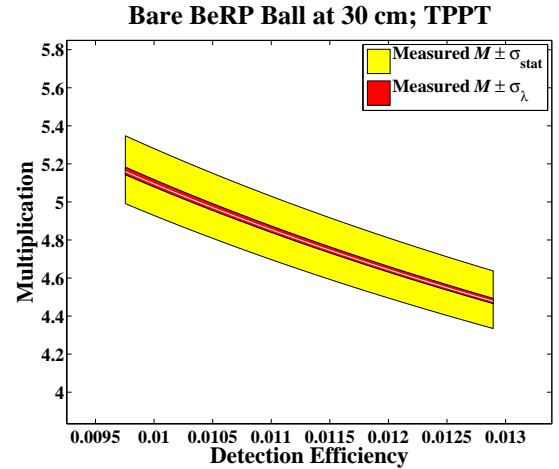


FIG. 10. Multiplication M vs. detection efficiency ϵ for the bare BeRP Ball 30 cm from the detector. The yellow contour represents the 1σ statistical errors (68.3% confidence region) in the measurements for the central value of λ . The red contour represents the 1σ errors in the measurements for the measured error in λ . The central value is noted by the white curve.

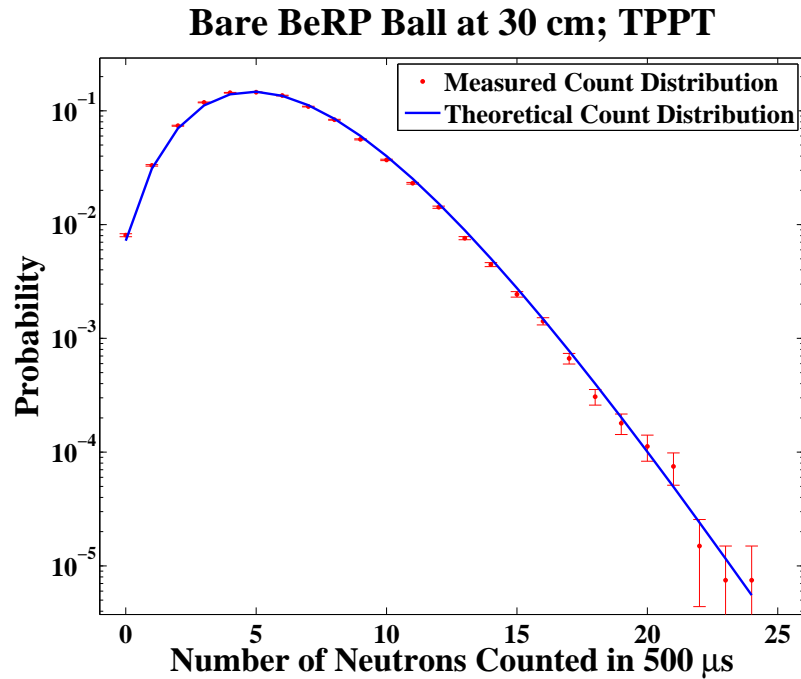


FIG. 11. Probability of counting n neutrons in a randomly-triggered time gate of duration $T = 500 \mu\text{s}$ for the bare BeRP Ball 30 cm from the detector.

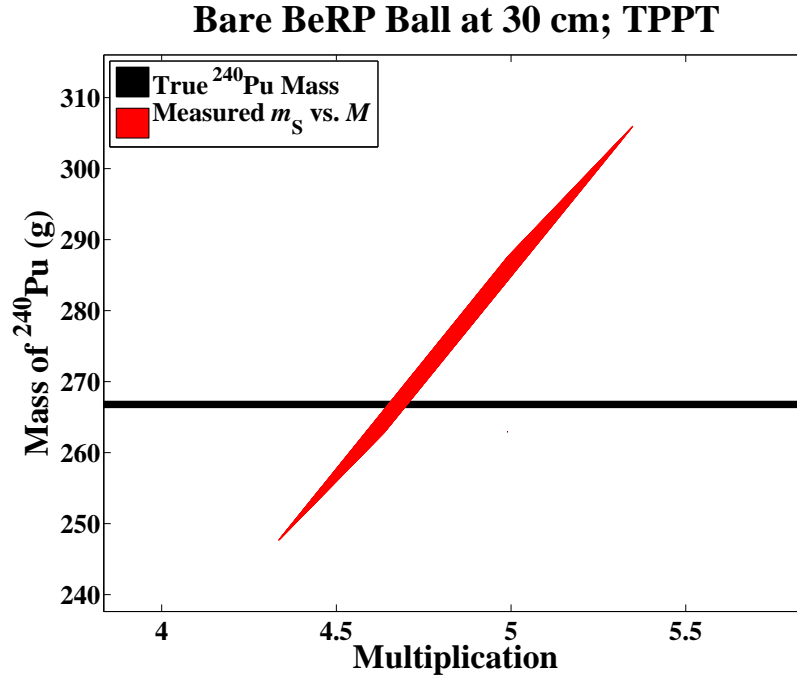


FIG. 12. Multiplication M vs. mass of ^{240}Pu for the bare BeRP Ball 30 cm from the detector. The red trapezoidal contour represents the 1σ error (68.3% confidence region) in the measurement. The true mass of $^{240}\text{Pu} = 266.8 \pm 0.5 \text{ g}$ and is indicated by the black horizontal line in the plot.

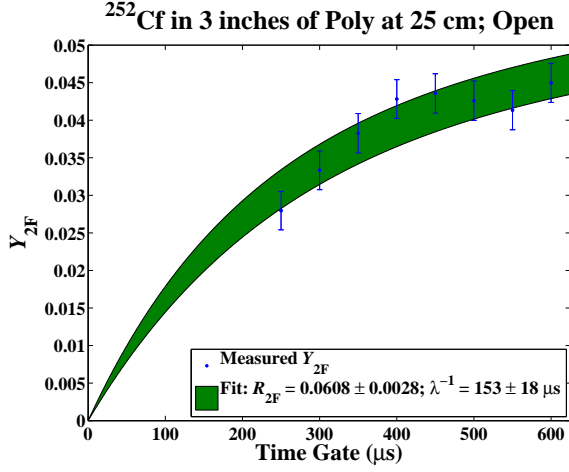


FIG. 13. Y_{2F} vs. time gate T for ^{252}Cf in 3 inch thick polyethylene 25 cm from the detector. The green contour represents the 1σ errors (68.3% confidence region) in the measurements.

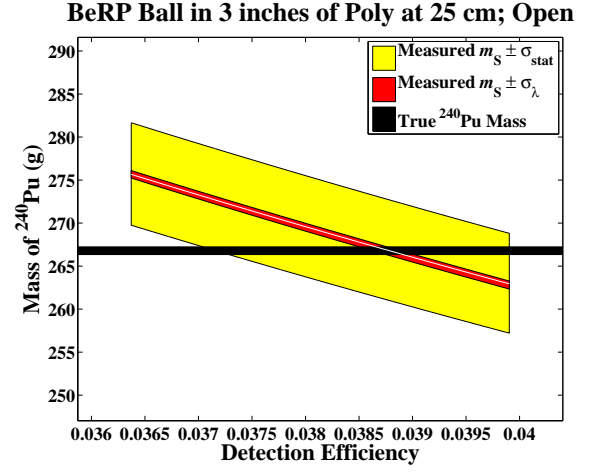


FIG. 15. Mass m_S of ^{240}Pu vs. detection efficiency ϵ for the BeRP Ball in 3 inch thick polyethylene 25 cm from the detector. The yellow contour represents the 1σ statistical errors (68.3% confidence region) in the measurements for the central value of λ . The red contour represents the 1σ errors in the measurements due to the measured error in λ . The central value is noted by the white curve. The true mass of $^{240}\text{Pu} = 266.8 \pm 0.5$ g and is indicated by the black horizontal line in the plot.

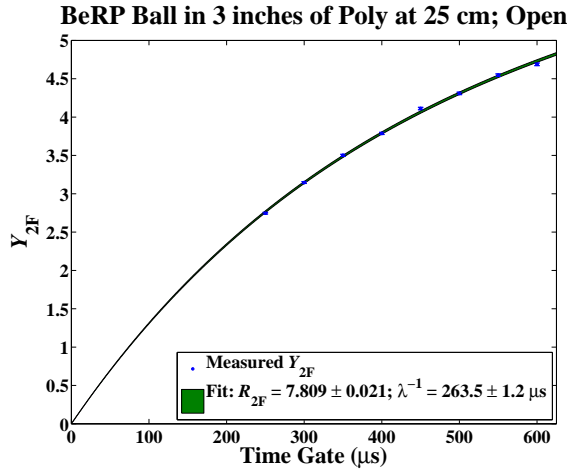


FIG. 14. Y_{2F} vs. time gate T for the BeRP Ball in 3 inch thick polyethylene 25 cm from the detector. The green contour represents the 1σ errors (68.3% confidence region) in the measurements.

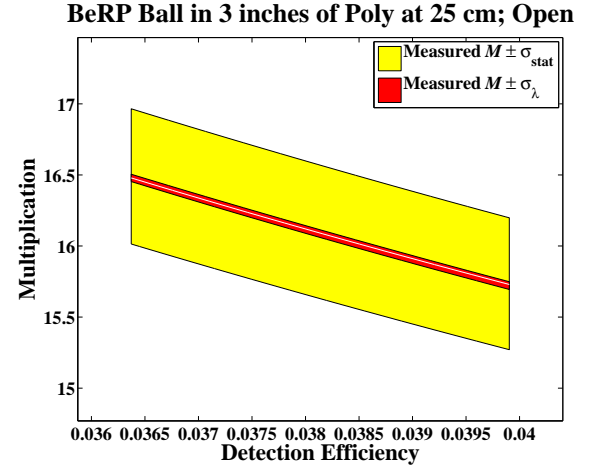


FIG. 16. Multiplication M vs. detection efficiency ϵ for the BeRP Ball in 3 inch thick polyethylene 25 cm from the detector. The yellow contour represents the 1σ statistical errors (68.3% confidence region) in the measurements for the central value of λ . The red contour represents the 1σ errors in the measurements for the measured error in λ . The central value is noted by the white curve.

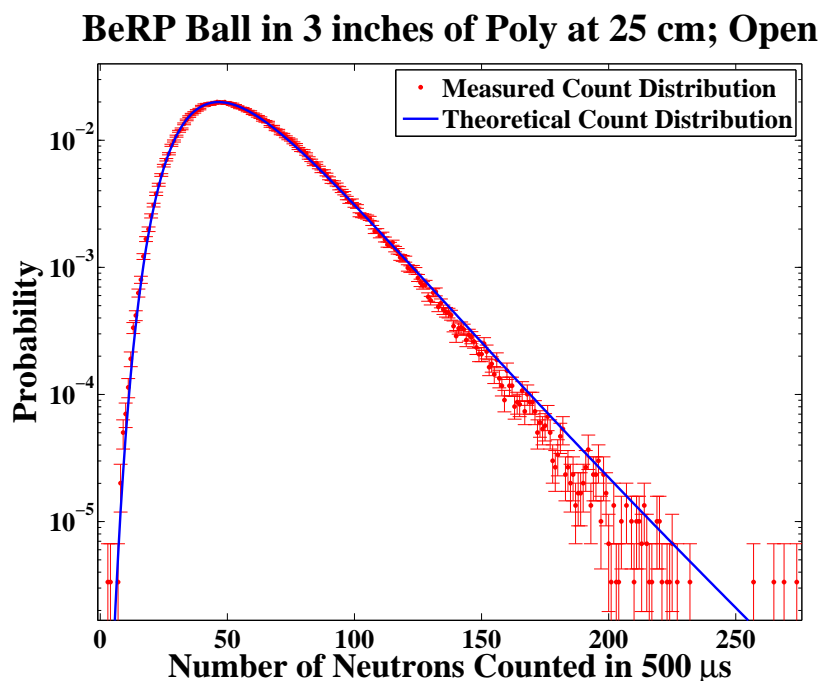


FIG. 17. Probability of counting n neutrons in a randomly-triggered time gate of duration $T = 500 \mu\text{s}$ for the BeRP Ball in 3 inch thick polyethylene 25 cm from the detector.

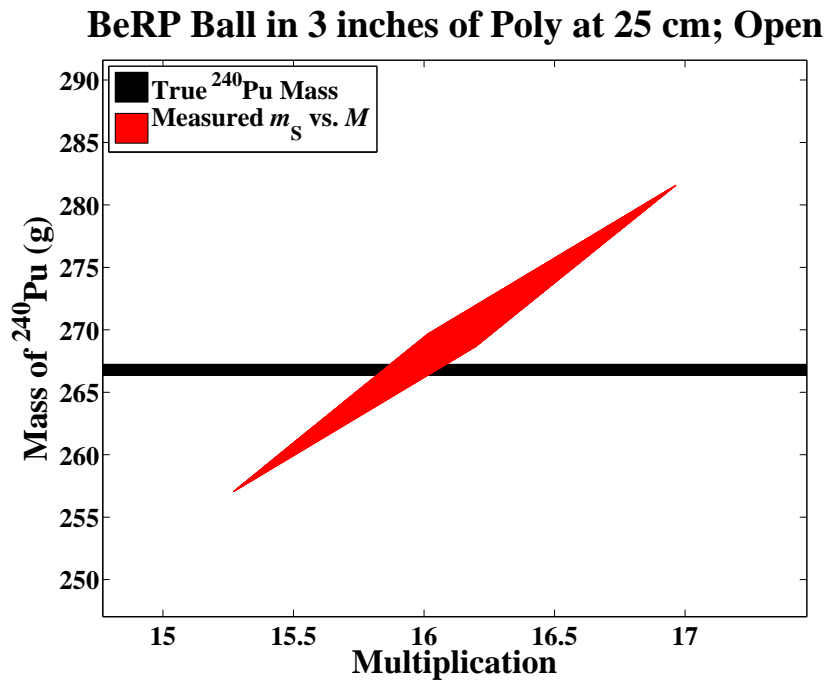


FIG. 18. Multiplication M vs. mass of ^{240}Pu for the BeRP Ball in 3 inch thick polyethylene 25 cm from the detector. The red trapezoidal contour represents the 1σ error (68.3% confidence region) in the measurement. The true mass of $^{240}\text{Pu} = 266.8 \pm 0.5$ g and is indicated by the black horizontal line in the plot.

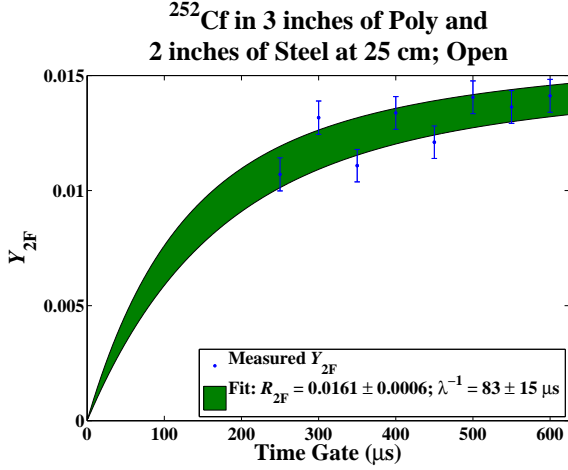


FIG. 19. Y_{2F} vs. time gate T for ^{252}Cf in 3 inch thick polyethylene and 2 inch thick steel 25 cm from the detector. The green contour represents the 1σ errors (68.3% confidence region) in the measurements.

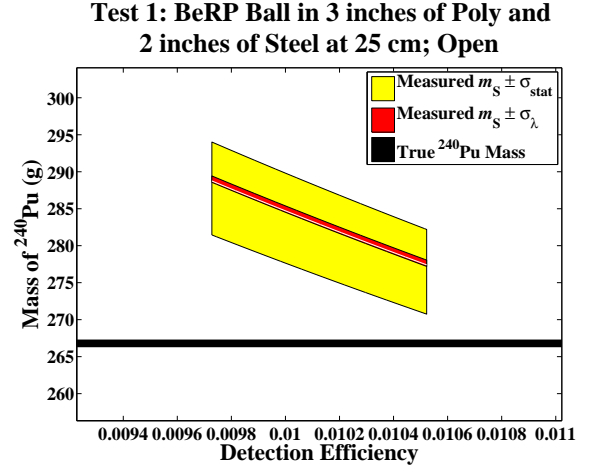


FIG. 21. Mass m_S of ^{240}Pu vs. detection efficiency ϵ for the BeRP Ball in 3 inch thick polyethylene and 2 inch thick steel 25 cm from the detector. The yellow contour represents the 1σ statistical errors (68.3% confidence region) in the measurements for the central value of λ . The red contour represents the 1σ errors in the measurements due to the measured error in λ . The central value is noted by the white curve. The true mass of $^{240}\text{Pu} = 266.8 \pm 0.5$ g and is indicated by the black horizontal line in the plot.

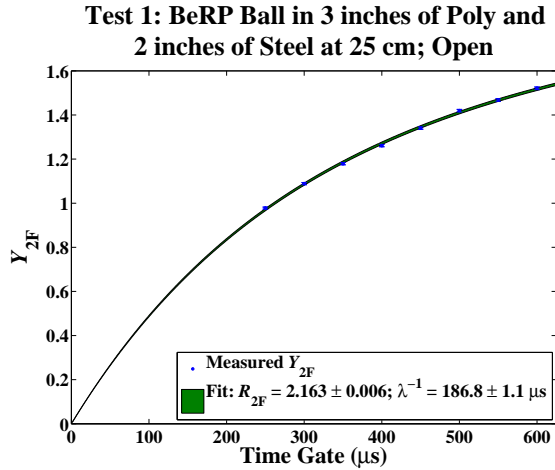


FIG. 20. Y_{2F} vs. time gate T for the BeRP Ball in 3 inch thick polyethylene and 2 inch thick steel 25 cm from the detector. The green contour represents the 1σ errors (68.3% confidence region) in the measurements.

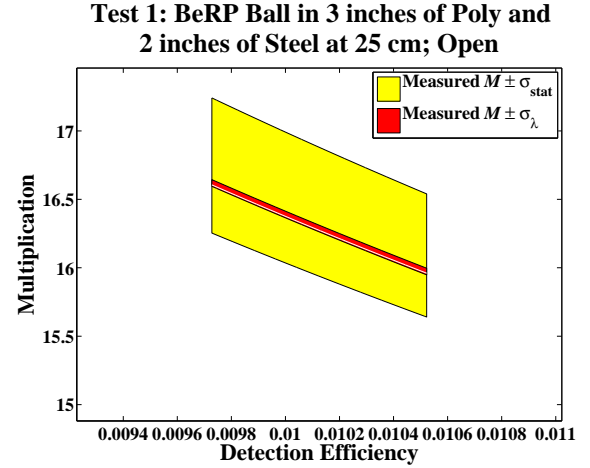


FIG. 22. Multiplication M vs. detection efficiency ϵ for the BeRP Ball in 3 inch thick polyethylene and 2 inch thick steel 25 cm from the detector. The yellow contour represents the 1σ statistical errors (68.3% confidence region) in the measurements for the central value of λ . The red contour represents the 1σ errors in the measurements for the measured error in λ . The central value is noted by the white curve.

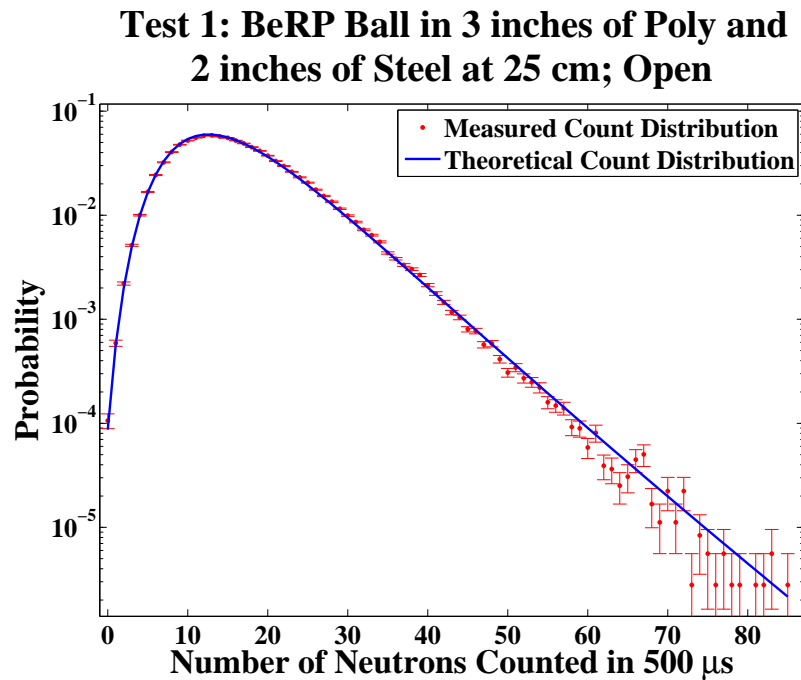


FIG. 23. Probability of counting n neutrons in a randomly-triggered time gate of duration $T = 500 \mu\text{s}$ for the BeRP Ball in 3 inch thick polyethylene and 2 inch thick steel 25 cm from the detector.

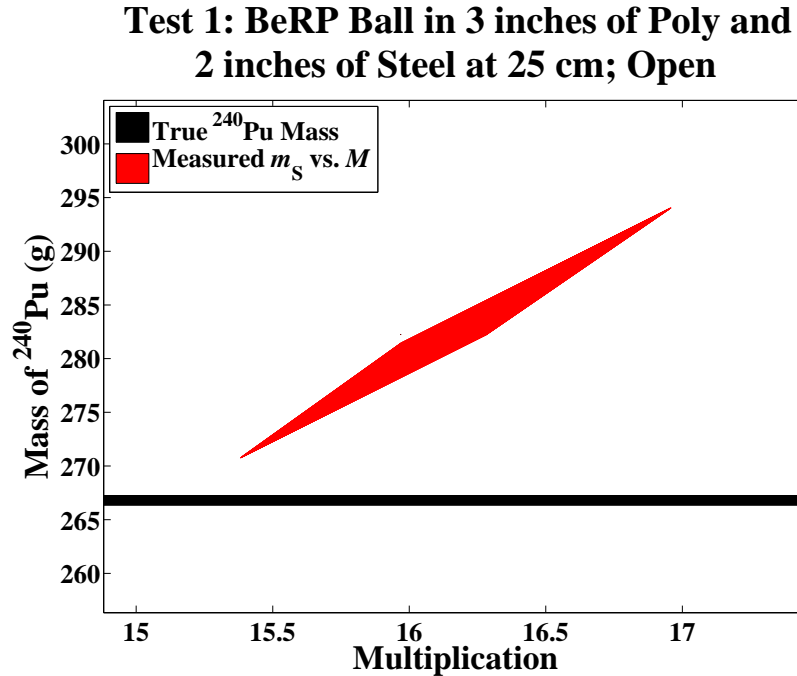


FIG. 24. Multiplication M vs. mass of ^{240}Pu for the BeRP Ball in 3 inch thick polyethylene and 2 inch thick steel 25 cm from the detector. The red trapezoidal contour represents the 1σ error (68.3% confidence region) in the measurement. The true mass of $^{240}\text{Pu} = 266.8 \pm 0.5 \text{ g}$ and is indicated by the black horizontal line in the plot.

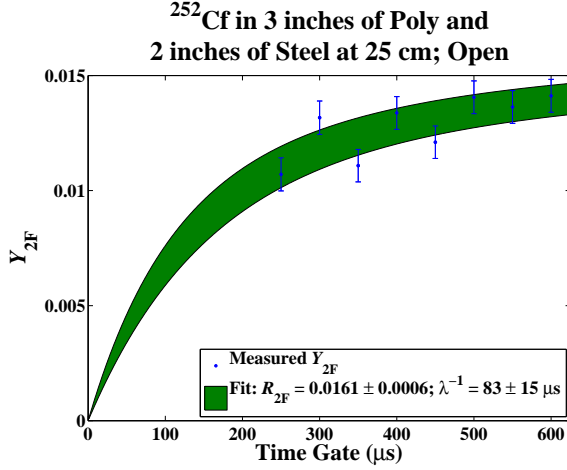


FIG. 25. Y_{2F} vs. time gate T for ^{252}Cf in 3 inch thick polyethylene and 2 inch thick steel 25 cm from the detector. The green contour represents the 1σ errors (68.3% confidence region) in the measurements.

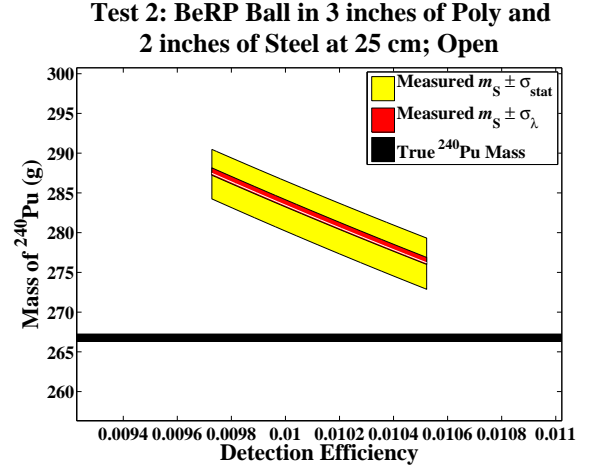


FIG. 27. Mass m_S of ^{240}Pu vs. detection efficiency ϵ for the BeRP Ball in 3 inch thick polyethylene and 2 inch thick steel 25 cm from the detector. The yellow contour represents the 1σ statistical errors (68.3% confidence region) in the measurements for the central value of λ . The red contour represents the 1σ errors in the measurements due to the measured error in λ . The central value is noted by the white curve. The true mass of $^{240}\text{Pu} = 266.8 \pm 0.5$ g and is indicated by the black horizontal line in the plot.

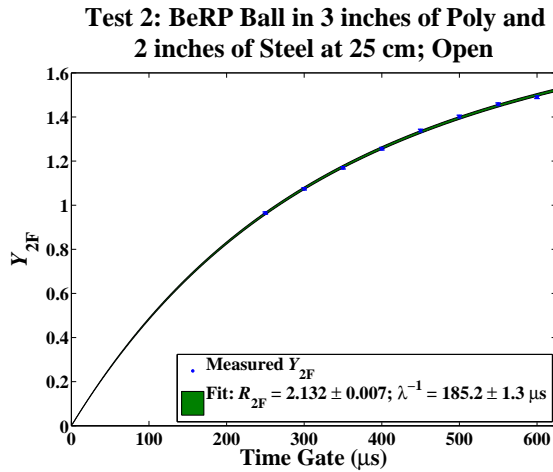


FIG. 26. Y_{2F} vs. time gate T for the BeRP Ball in 3 inch thick polyethylene and 2 inch thick steel 25 cm from the detector. The green contour represents the 1σ errors (68.3% confidence region) in the measurements.

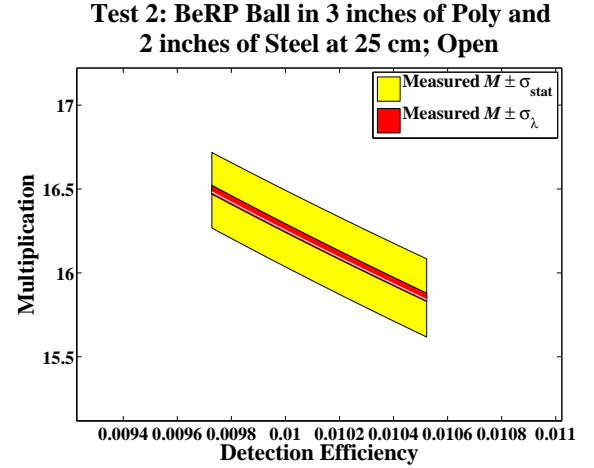


FIG. 28. Multiplication M vs. detection efficiency ϵ for the BeRP Ball in 3 inch thick polyethylene and 2 inch thick steel 25 cm from the detector. The yellow contour represents the 1σ statistical errors (68.3% confidence region) in the measurements for the central value of λ . The red contour represents the 1σ errors in the measurements for the measured error in λ . The central value is noted by the white curve.

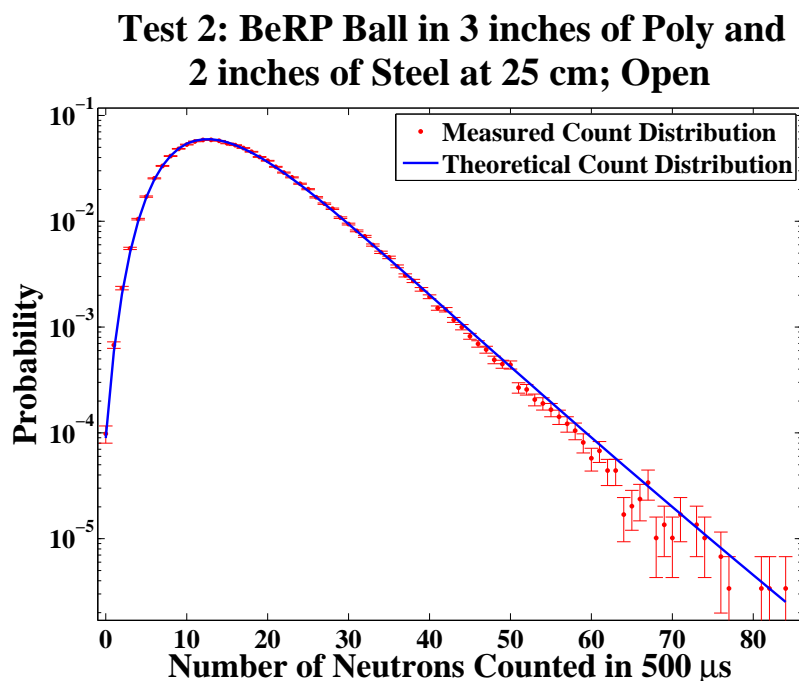


FIG. 29. Probability of counting n neutrons in a randomly-triggered time gate of duration $T = 500 \mu\text{s}$ for the BeRP Ball in 3 inch thick polyethylene and 2 inch thick steel 25 cm from the detector.

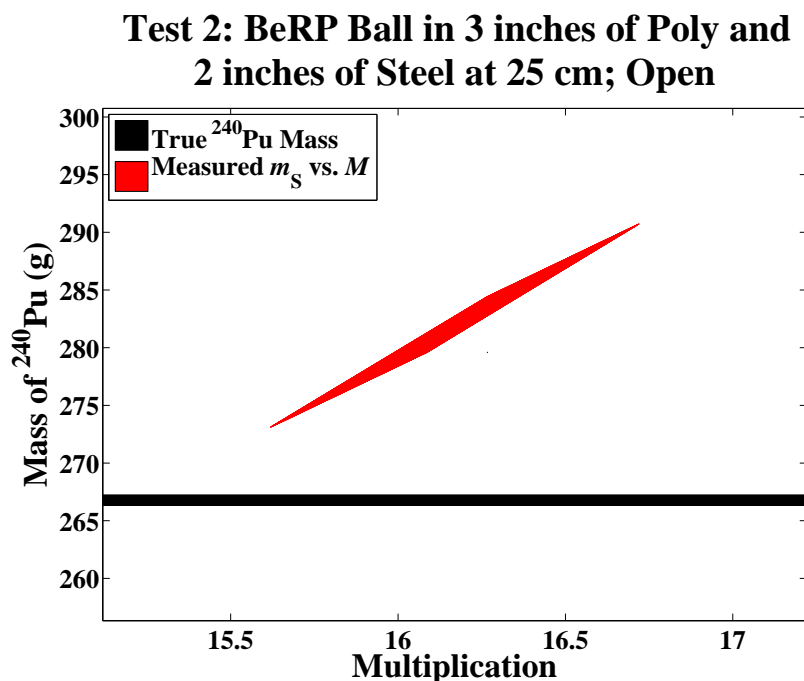


FIG. 30. Multiplication M vs. mass of ^{240}Pu for the BeRP Ball in 3 inch thick polyethylene and 2 inch thick steel 25 cm from the detector. The red trapezoidal contour represents the 1σ error (68.3% confidence region) in the measurement. The true mass of $^{240}\text{Pu} = 266.8 \pm 0.5$ g and is indicated by the black horizontal line in the plot.

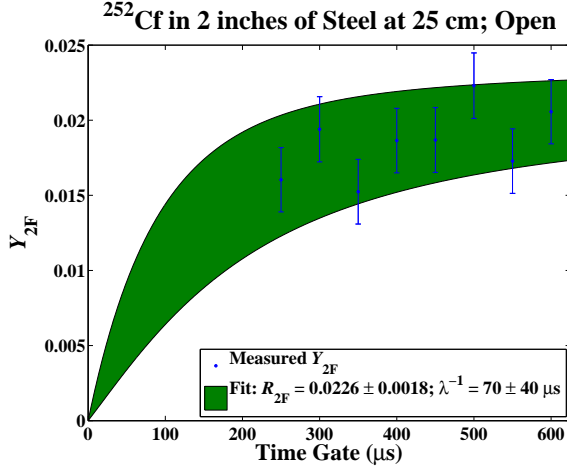


FIG. 31. Y_{2F} vs. time gate T for ^{252}Cf in 2 inch thick steel 25 cm from the detector. The green contour represents the 1σ errors (68.3% confidence region) in the measurements.

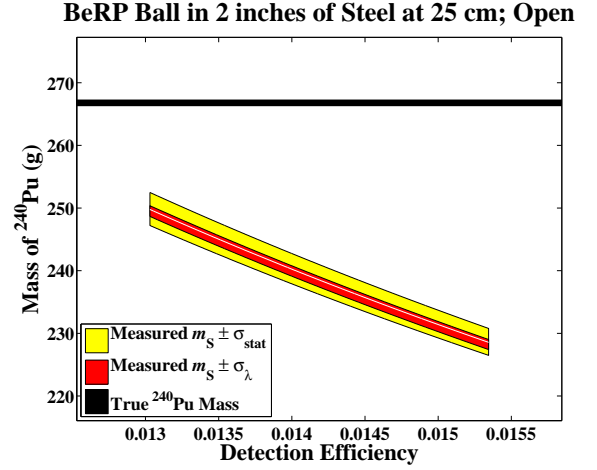


FIG. 33. Mass m_S of ^{240}Pu vs. detection efficiency ϵ for the BeRP Ball in 2 inch thick steel 25 cm from the detector. The yellow contour represents the 1σ statistical errors (68.3% confidence region) in the measurements for the central value of λ . The red contour represents the 1σ errors in the measurements due to the measured error in λ . The central value is noted by the white curve. The true mass of $^{240}\text{Pu} = 266.8 \pm 0.5$ g and is indicated by the black horizontal line in the plot.

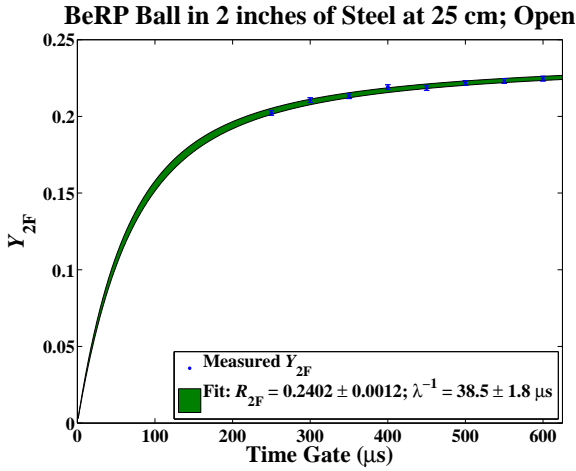


FIG. 32. Y_{2F} vs. time gate T for the BeRP Ball in 2 inch thick steel 25 cm from the detector. The green contour represents the 1σ errors (68.3% confidence region) in the measurements.

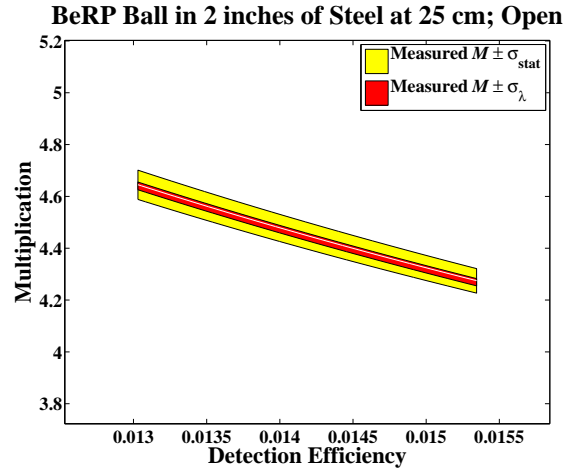


FIG. 34. Multiplication M vs. detection efficiency ϵ for the BeRP Ball in 2 inch thick steel 25 cm from the detector. The yellow contour represents the 1σ statistical errors (68.3% confidence region) in the measurements for the central value of λ . The red contour represents the 1σ errors in the measurements for the measured error in λ . The central value is noted by the white curve.

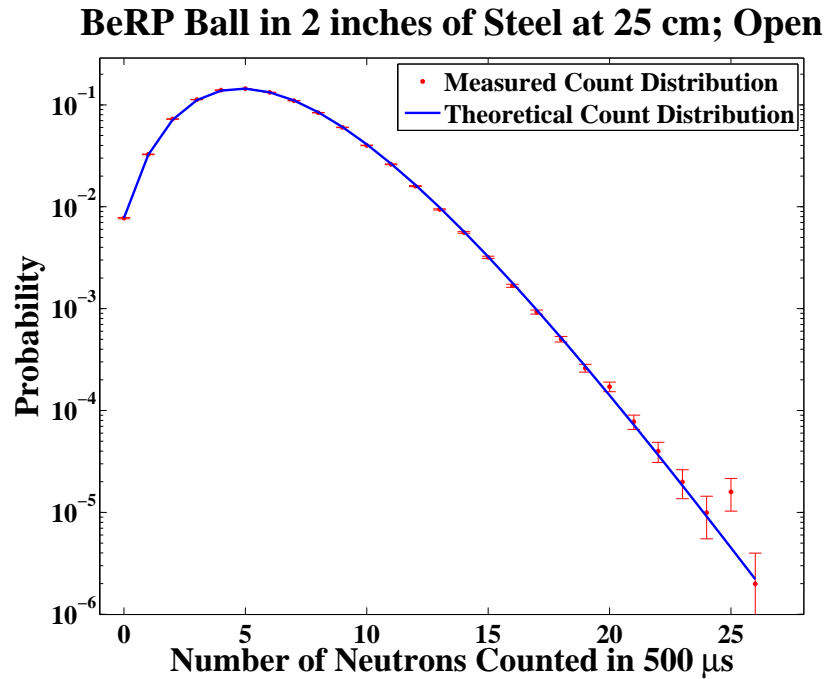


FIG. 35. Probability of counting n neutrons in a randomly-triggered time gate of duration $T = 500 \mu\text{s}$ for the BeRP Ball in 2 inch thick steel 25 cm from the detector.

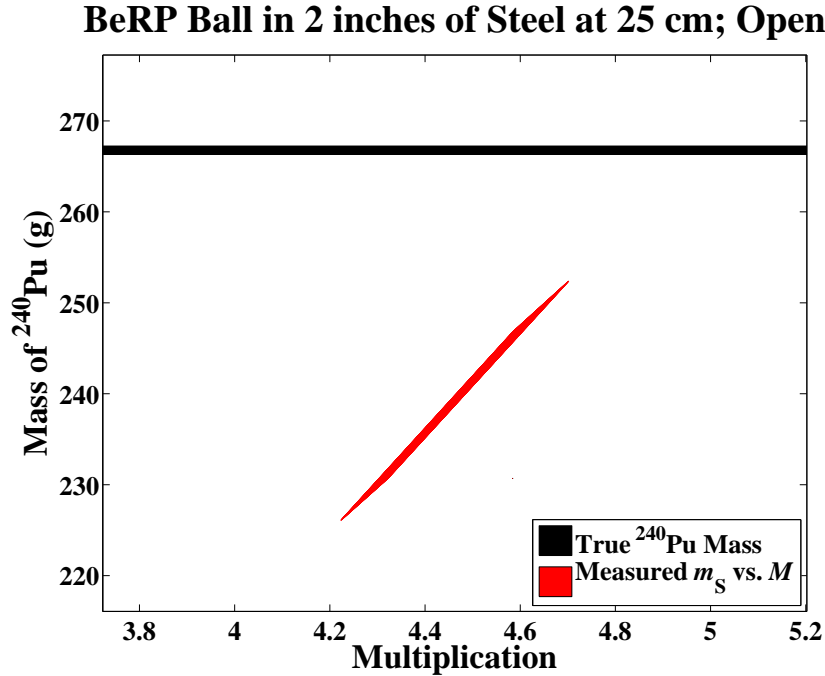


FIG. 36. Multiplication M vs. mass of ^{240}Pu for the BeRP Ball in 2 inch thick steel 25 cm from the detector. The red trapezoidal contour represents the 1σ error (68.3% confidence region) in the measurement. The true mass of $^{240}\text{Pu} = 266.8 \pm 0.5 \text{ g}$ and is indicated by the black horizontal line in the plot.

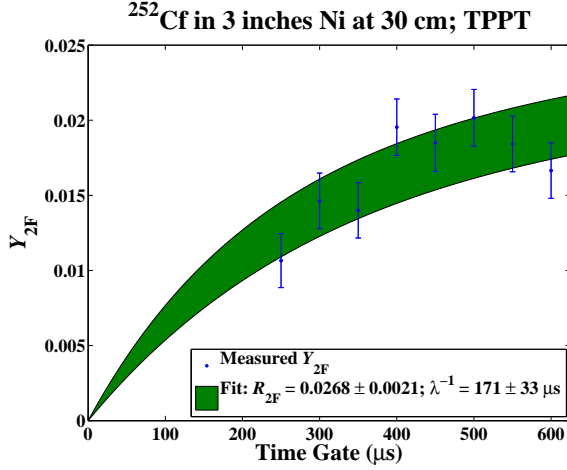


FIG. 37. Y_{2F} vs. time gate T for ^{252}Cf in 3 inch thick nickel 30 cm from the detector. The green contour represents the 1σ errors (68.3% confidence region) in the measurements.

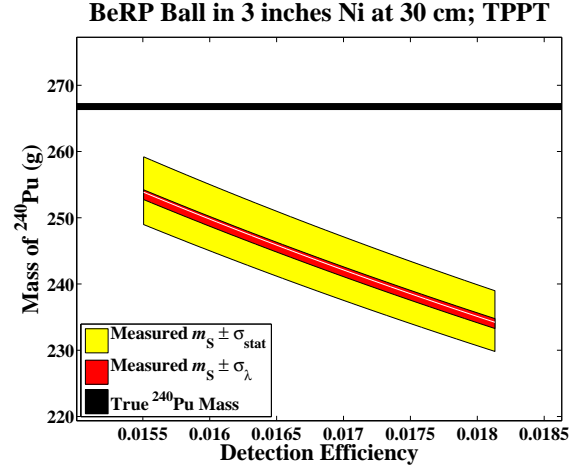


FIG. 39. Mass m_S of ^{240}Pu vs. detection efficiency ϵ for the BeRP Ball in 3 inch thick nickel 30 cm from the detector. The yellow contour represents the 1σ statistical errors (68.3% confidence region) in the measurements for the central value of λ . The red contour represents the 1σ errors in the measurements due to the measured error in λ . The central value is noted by the white curve. The true mass of $^{240}\text{Pu} = 266.8 \pm 0.5$ g and is indicated by the black horizontal line in the plot.

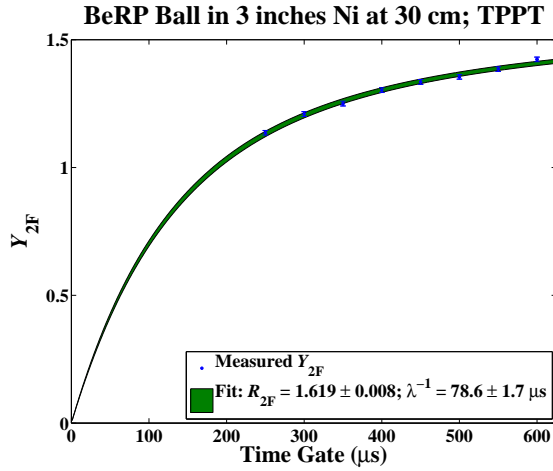


FIG. 38. Y_{2F} vs. time gate T for the BeRP Ball in 3 inch thick nickel 30 cm from the detector. The green contour represents the 1σ errors (68.3% confidence region) in the measurements.

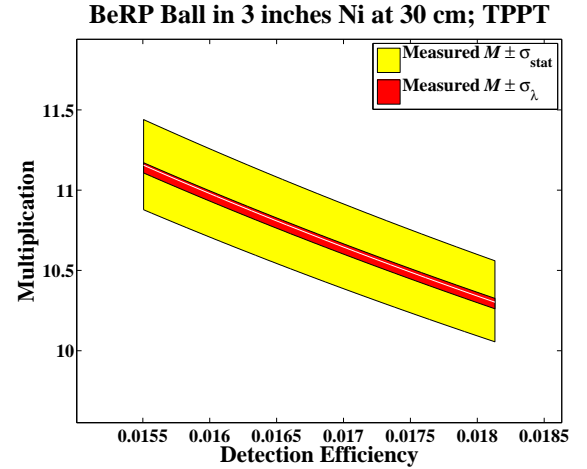


FIG. 40. Multiplication M vs. detection efficiency ϵ for the BeRP Ball in 3 inch thick nickel 30 cm from the detector. The yellow contour represents the 1σ statistical errors (68.3% confidence region) in the measurements for the central value of λ . The red contour represents the 1σ errors in the measurements for the measured error in λ . The central value is noted by the white curve.

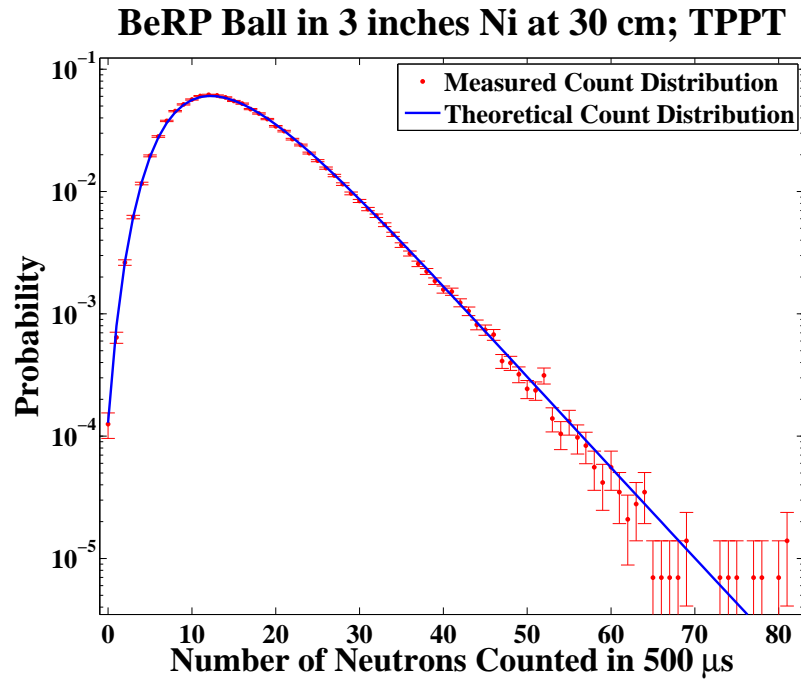


FIG. 41. Probability of counting n neutrons in a randomly-triggered time gate of duration $T = 500 \mu\text{s}$ for the BeRP Ball in 3 inch thick nickel 30 cm from the detector.

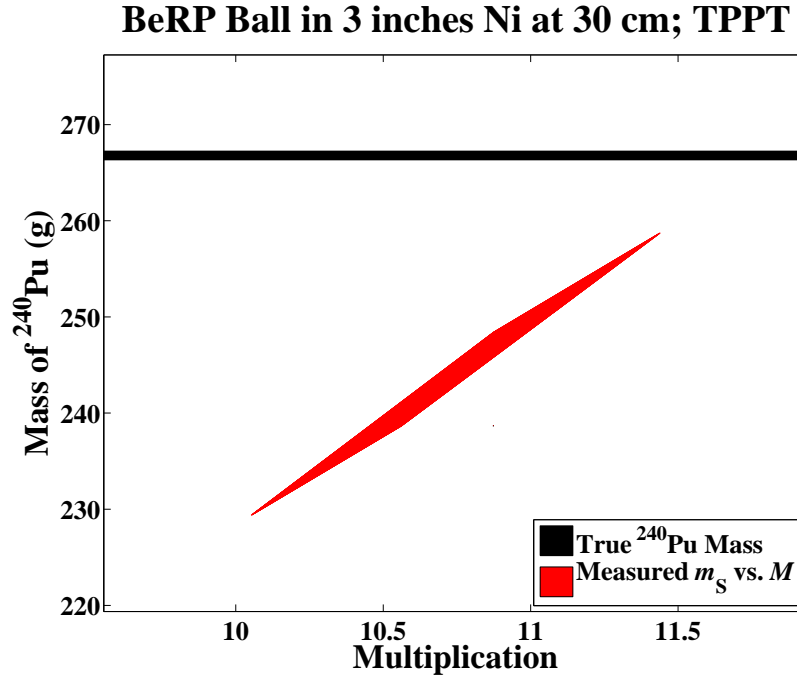


FIG. 42. Multiplication M vs. mass of ^{240}Pu for the BeRP Ball in 3 inch thick nickel 30 cm from the detector. The red trapezoidal contour represents the 1σ error (68.3% confidence region) in the measurement. The true mass of $^{240}\text{Pu} = 266.8 \pm 0.5$ g and is indicated by the black horizontal line in the plot.

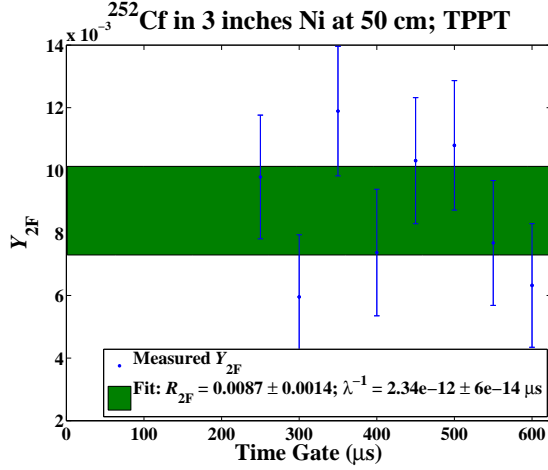


FIG. 43. Y_{2F} vs. time gate T for ^{252}Cf in 3 inch thick nickel 50 cm from the detector. The green contour represents the 1σ errors (68.3% confidence region) in the measurements.

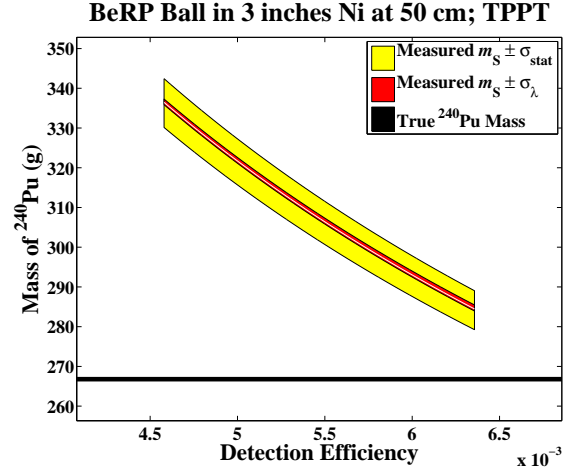


FIG. 45. Mass m_s of ^{240}Pu vs. detection efficiency ϵ for the BeRP Ball in 3 inch thick nickel 50 cm from the detector. The yellow contour represents the 1σ statistical errors (68.3% confidence region) in the measurements for the central value of λ . The red contour represents the 1σ errors in the measurements due to the measured error in λ . The central value is noted by the white curve. The true mass of $^{240}\text{Pu} = 266.8 \pm 0.5$ g and is indicated by the black horizontal line in the plot.

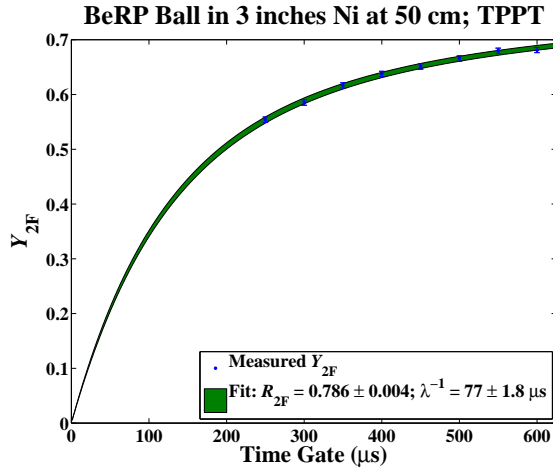


FIG. 44. Y_{2F} vs. time gate T for the BeRP Ball in 3 inch thick nickel 50 cm from the detector. The green contour represents the 1σ errors (68.3% confidence region) in the measurements.

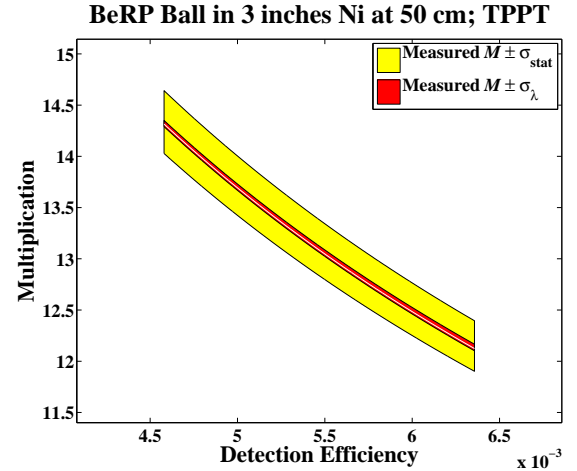


FIG. 46. Multiplication M vs. detection efficiency ϵ for the BeRP Ball in 3 inch thick nickel 50 cm from the detector. The yellow contour represents the 1σ statistical errors (68.3% confidence region) in the measurements for the central value of λ . The red contour represents the 1σ errors in the measurements for the measured error in λ . The central value is noted by the white curve.

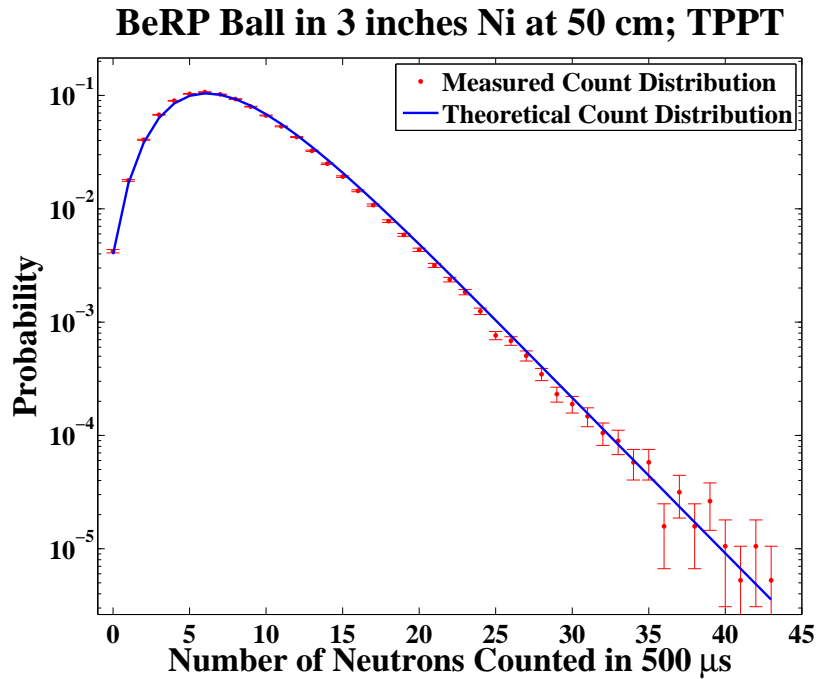


FIG. 47. Probability of counting n neutrons in a randomly-triggered time gate of duration $T = 500 \mu\text{s}$ for the BeRP Ball in 3 inch thick nickel 50 cm from the detector.

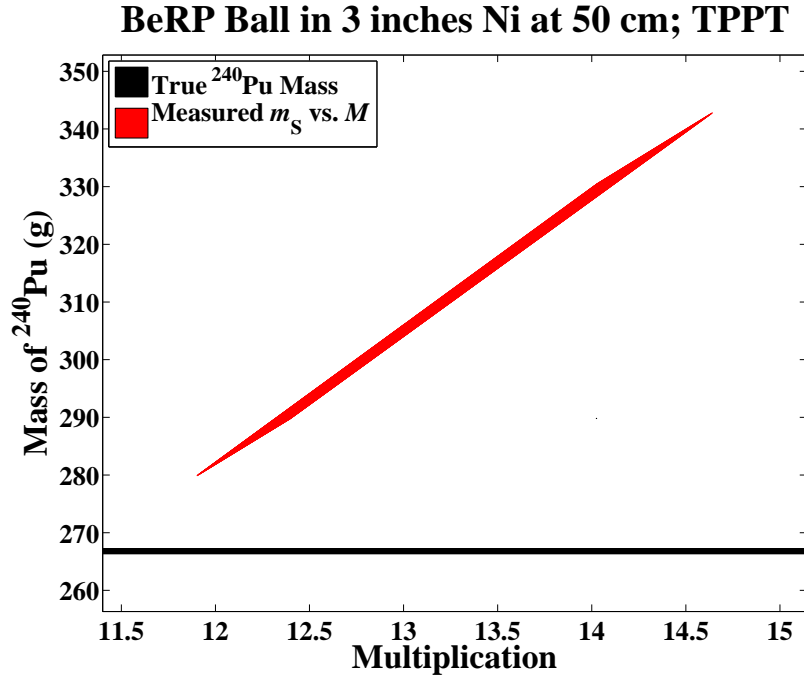


FIG. 48. Multiplication M vs. mass of ^{240}Pu for the BeRP Ball in 3 inch thick nickel 50 cm from the detector. The red trapezoidal contour represents the 1σ error (68.3% confidence region) in the measurement. The true mass of $^{240}\text{Pu} = 266.8 \pm 0.5$ g and is indicated by the black horizontal line in the plot.

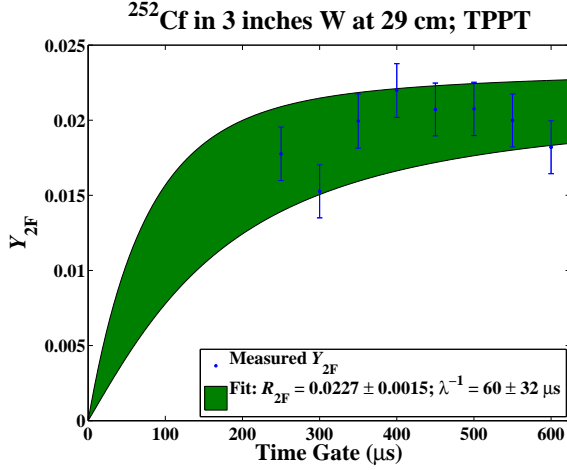


FIG. 49. Y_{2F} vs. time gate T for ^{252}Cf in 3 inch thick tungsten 29 cm from the detector. The green contour represents the 1σ errors (68.3% confidence region) in the measurements.

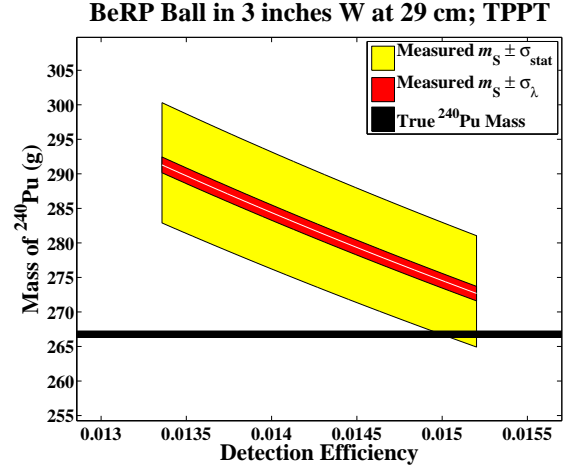


FIG. 51. Mass m_s of ^{240}Pu vs. detection efficiency ϵ for the BeRP Ball in 3 inch thick tungsten 29 cm from the detector. The yellow contour represents the 1σ statistical errors (68.3% confidence region) in the measurements for the central value of λ . The red contour represents the 1σ errors in the measurements due to the measured error in λ . The central value is noted by the white curve. The true mass of $^{240}\text{Pu} = 266.8 \pm 0.5$ g and is indicated by the black horizontal line in the plot.

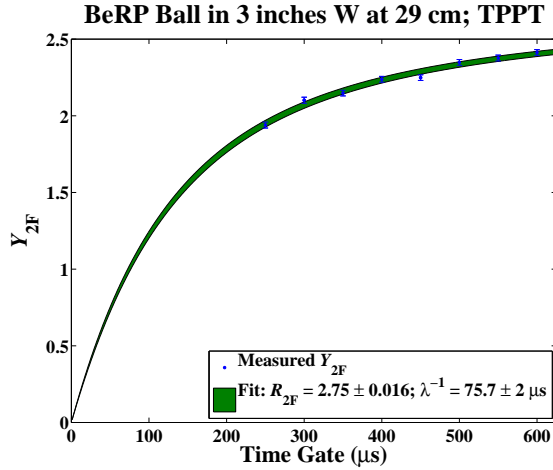


FIG. 50. Y_{2F} vs. time gate T for the BeRP Ball in 3 inch thick tungsten 29 cm from the detector. The green contour represents the 1σ errors (68.3% confidence region) in the measurements.

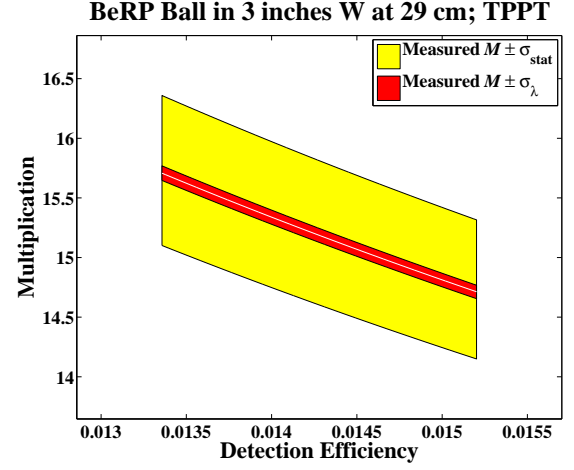


FIG. 52. Multiplication M vs. detection efficiency ϵ for the BeRP Ball in 3 inch thick tungsten 29 cm from the detector. The yellow contour represents the 1σ statistical errors (68.3% confidence region) in the measurements for the central value of λ . The red contour represents the 1σ errors in the measurements for the measured error in λ . The central value is noted by the white curve.

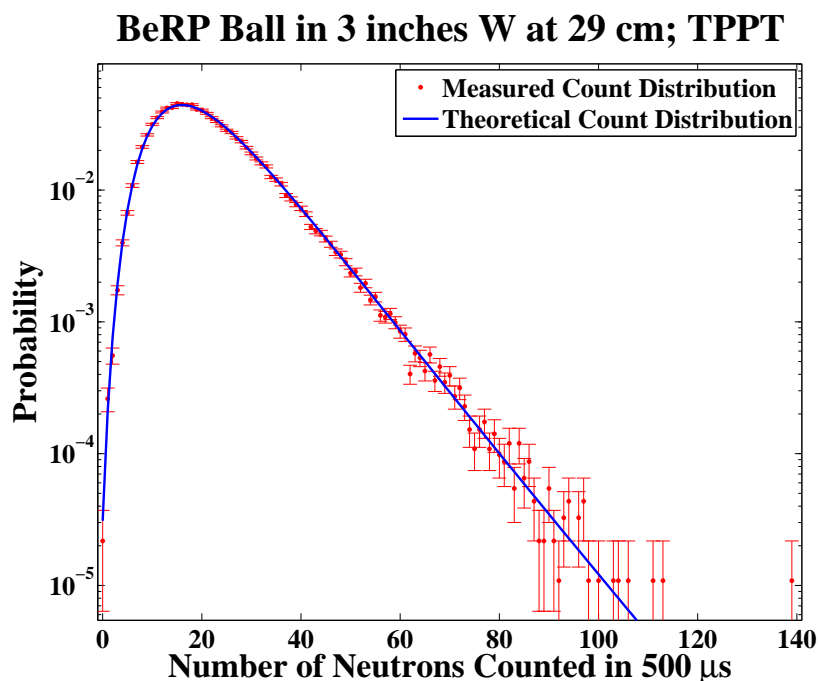


FIG. 53. Probability of counting n neutrons in a randomly-triggered time gate of duration $T = 500 \mu\text{s}$ for the BeRP Ball in 3 inch thick tungsten 29 cm from the detector.

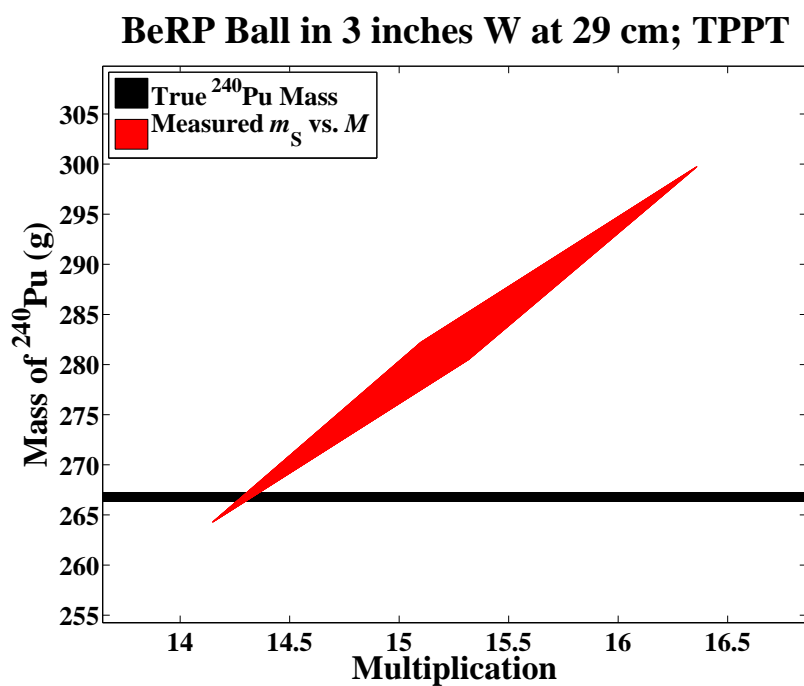


FIG. 54. Multiplication M vs. mass of ^{240}Pu for the BeRP Ball in 3 inch thick tungsten 29 cm from the detector. The red trapezoidal contour represents the 1σ error (68.3% confidence region) in the measurement. The true mass of $^{240}\text{Pu} = 266.8 \pm 0.5$ g and is indicated by the black horizontal line in the plot.

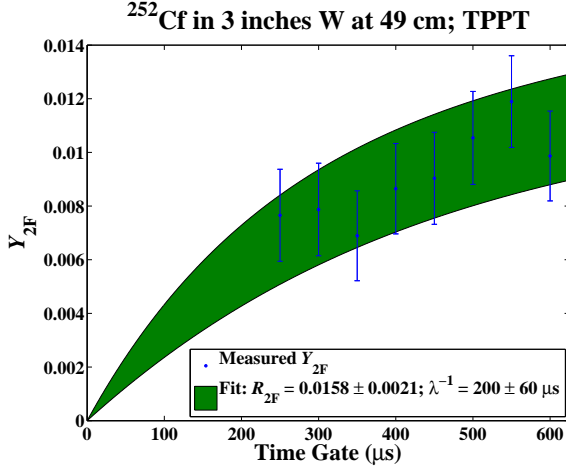


FIG. 55. Y_{2F} vs. time gate T for ^{252}Cf in 3 inch thick tungsten 49 cm from the detector. The green contour represents the 1σ errors (68.3% confidence region) in the measurements.

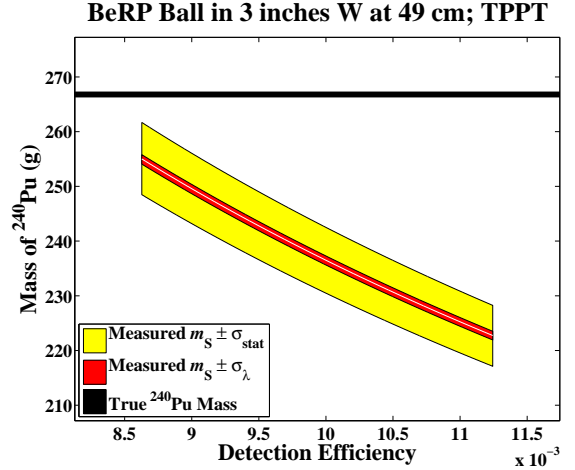


FIG. 57. Mass m_S of ^{240}Pu vs. detection efficiency ϵ for the BeRP Ball in 3 inch thick tungsten 49 cm from the detector. The yellow contour represents the 1σ statistical errors (68.3% confidence region) in the measurements for the central value of λ . The red contour represents the 1σ errors in the measurements due to the measured error in λ . The central value is noted by the white curve. The true mass of $^{240}\text{Pu} = 266.8 \pm 0.5$ g and is indicated by the black horizontal line in the plot.

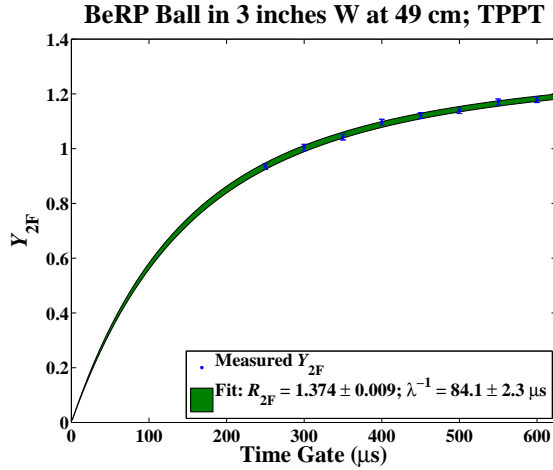


FIG. 56. Y_{2F} vs. time gate T for the BeRP Ball in 3 inch thick tungsten 49 cm from the detector. The green contour represents the 1σ errors (68.3% confidence region) in the measurements.

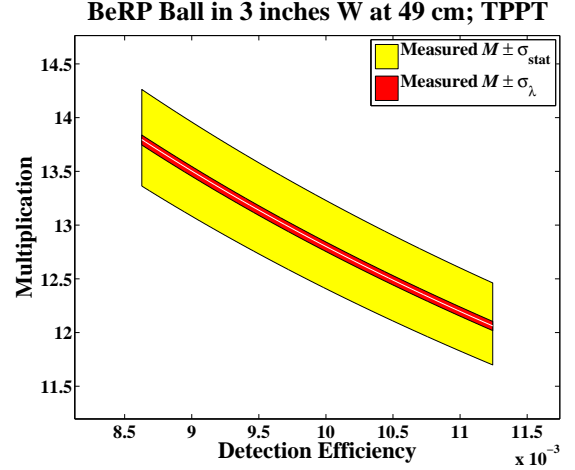


FIG. 58. Multiplication M vs. detection efficiency ϵ for the BeRP Ball in 3 inch thick tungsten 49 cm from the detector. The yellow contour represents the 1σ statistical errors (68.3% confidence region) in the measurements for the central value of λ . The red contour represents the 1σ errors in the measurements for the measured error in λ . The central value is noted by the white curve.

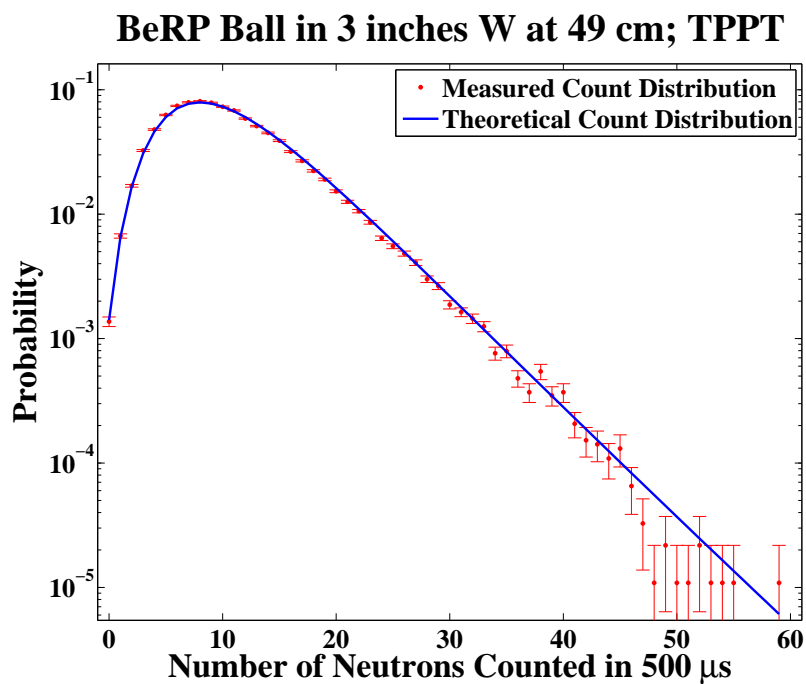


FIG. 59. Probability of counting n neutrons in a randomly-triggered time gate of duration $T = 500 \mu\text{s}$ for the BeRP Ball in 3 inch thick tungsten 49 cm from the detector.

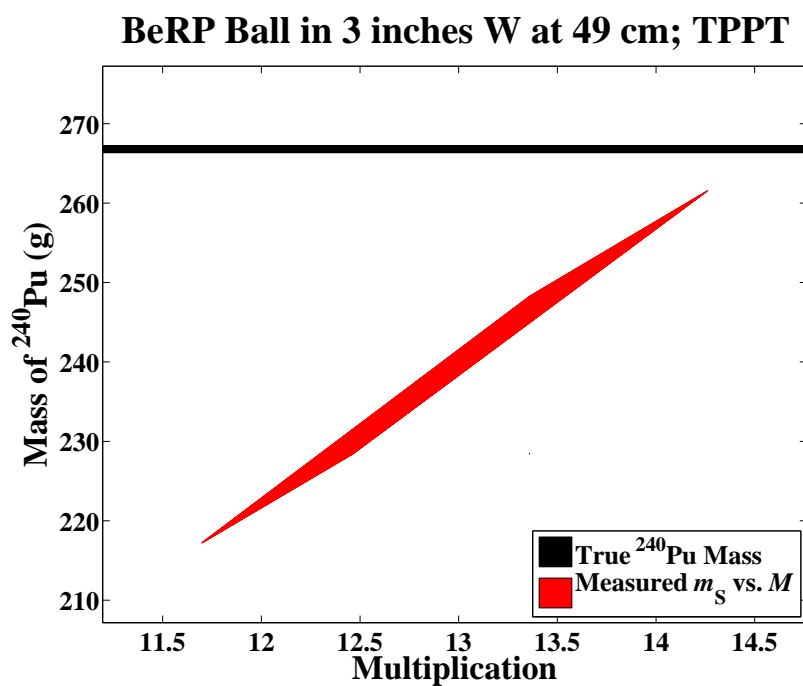


FIG. 60. Multiplication M vs. mass of ^{240}Pu for the BeRP Ball in 3 inch thick tungsten 49 cm from the detector. The red trapezoidal contour represents the 1σ error (68.3% confidence region) in the measurement. The true mass of $^{240}\text{Pu} = 266.8 \pm 0.5$ g and is indicated by the black horizontal line in the plot.

Mass m_S of ^{240}Pu (g)	Scale factor	Reflector	Thickness (inches)	k_{eff}	Scale factor	M	Scale factor	M_E	Scale factor
267 ± 7	$S = 1.4$	None	0	0.779 ± 0.018		4.45 ± 0.35		3.3 ± 0.24	
		Polyethylene	3	0.9380 ± 0.0033		16.1 ± 0.8		11.1 ± 0.6	
		Polyethylene, Steel	3, 2	0.9382 ± 0.0018		16.2 ± 0.5		11.1 ± 0.33	
		Steel	2	0.776 ± 0.012		4.46 ± 0.24		3.31 ± 0.16	
		Nickel	3	0.913 ± 0.009	$S = 1.8$	11.2 ± 1.0	$S = 1.7$	7.9 ± 0.7	$S = 1.7$
		Tungsten	3	0.931 ± 0.005	$S = 1.2$	14.3 ± 1.1	$S = 1.4$	9.9 ± 0.7	$S = 1.3$

TABLE VI. Combined measurements of the BeRP Ball in various reflectors. Combined measurements of the mass of ^{240}Pu m_S , k_{eff} , multiplication M , and the escape multiplication M_E are listed.

V. CONCLUSIONS

These measurements came reasonably close to reproducing the known mass m_S of ^{240}Pu in the BeRP Ball. The combined measurement gave $m_S = 267 \pm 7$ grams which compared very favorably to the known value from isotopics of $m_S = 266.8 \pm 0.5$. This proximity gives additional credence to the measured values for k_{eff} , multiplication M , and escape multiplication M_E shown in Table VI.

VI. REFERENCES

- ¹R. Sanchez, "Plutonium sphere surrounded by highly enriched uranium," (2005), MIX-MET-FAST-013.
- ²M. Rowland and R. Alvarez, "Real-time multiplicity counter," United States Patent No. 7,755,0165.
- ³M. Rowland and N. Snyderman, "Fissionmeter," United States Patent No. 8,155,258 B2.
- ⁴<http://www.ortec-online.com/solutions/neutron-detection-instruments-systems.aspx>.
- ⁵H. S. Wilf, *generatingfunctionology* (Academic Press, Inc., 1994).
- ⁶K. Böhnel, "The effect of multiplication on the quantitative determination of spontaneously fissioning isotopes by neutron correlation analysis," Nucl. Sci. Eng. **90**, 75 (1985).
- ⁷M. K. Prasad and N. J. Snyderman, "Statistical theory of fission chains and generalized poisson neutron counting distributions," Nucl. Sci. Eng. **172**, 300 (2012).
- ⁸J. Matthews and R. L. Walker, *Mathematical Methods of Physics, Second Edition* (Addison-Wesley Publishing Company, Inc., Menlo Park, 1970).
- ⁹W. Hage and D. M. Cifarelli, "Correlation analysis with neutron count distributions in randomly or signal triggered time intervals for assay of special fissile materials," Nucl. Sci. Eng. **89**, 159 (1985).
- ¹⁰K. Nakamura et al. (Particle Data Group), "Review of particle physics," J. Phys. **G 37**, 075021 (2010).
- ¹¹G. Cowan, *Statistical Data Analysis* (Oxford University Press Inc., New York, 1998).
- ¹²M. Abramowitz and I. Stegun, *Handbook of Mathematical Functions with Formulas, Graphs, and Mathematical Tables* (Dover Publications, New York, 1972).
- ¹³R. P. Feynman, "Statistical behavior of neutron chains," (1946), Los Alamos Report LA-591 (Classified).
- ¹⁴F. de Hoffman, *The Science and Engineering of Nuclear Power*, Vol. II (Addison Wesley Press, Cambridge, MA, 1949).
- ¹⁵R. P. Feynman, F. de Hoffman, and R. Serber, "Dispersion of the neutron emission in U-235 fission," Journal of Nuclear Energy **3**, 64–69 (1956).
- ¹⁶W. Hage and D. M. Cifarelli, "Models for a three-parameter analysis of neutron signal correlation measurements for fissile material assay," Nucl. Instr. and Meth. **A251**, 550–563 (1986).
- ¹⁷J. M. Verbeke, C. Hagmann, and D. Wright, "Simulation of neutron and gamma ray emission from fission and photofission," Tech. Rep. UCRL-AR-228518 (2010).
- ¹⁸R. R. Spencer, R. Gwin, and R. Ingle, "Measurement of the average number of prompt neutrons from spontaneous fission of californium-252," Nucl. Sci. Eng. **80**, 603–629 (1982).
- ¹⁹J. W. Boldeman and M. G. Hines, "Prompt neutron emission probabilities following spontaneous and thermal neutron fission," Nucl. Sci. Eng. **91** (1985).
- ²⁰*International Conference on Nuclear Data for Basic and Applied Science (Proceedings)* (Santa Fe, New Mexico, 1985).